A meta-analysis of thermo-physical and chemical aspects in CFD modelling of pyrolysis of a single wood particle in the thermally thick regime

Przemyslaw Maziarka[1,2*], Andrés Anca-Couce[3,4], Wolter Prins[1], Frederik Ronsse[1]

[1] Department of Green Chemistry and Technology, Faculty of Bioscience Engineering, Ghent University, Coupure Links 653, 9000 Gent, Belgium

[2] Department of Conversion Technologies of Biobased Resources, Institute of Agricultural Engineering, University of Hohenheim, Garbenstrasse 9, 70599 Stuttgart, Germany

[3] Division of Sustainable, clean and bioenergy systems, Institute of Thermal Engineering, Graz University of Technology, Inffeldgasse 25/B, 8010 Graz, Austria

[4] Thermal and Fluids Engineering Department, Carlos III University of Madrid, Avda. de la Universidad 30, 28911 Leganés, Madrid, Spain

* Corresponding author: Przemyslaw.Maziarka@UGent.be

Abstract

Thermochemical conversion of larger biomass particles (thermally thick regime) toward high-end products still suffers from an unrevealed quantitative relationship between process and product parameters. The main issue relates to the influence of heating rate within the particle, critical conversion-wise but difficult to assess experimentally. Computational fluid dynamics (CFD) modelling may help, but first the model must prove its reliability to prevent error transfer to the results. This study aimed to provide an unbiased, state-of-the-art model constructed in a stepwise mode to investigate the heating rate's distribution. Several datasets with broadly varying parameters from the literature were used for the development and validation since the reproduction of datasets would not bring novelty to solving the problem. Instead of the model's calibration to fit to the data, the parameters for each step-model were meticulously selected to match the experimental conditions. The stepwise development showed the best accuracy when the anisotropy and the heat sink drying sub-model were implemented. Moreover, using the Ranzi-Anca-Couce (RAC) scheme led to more accurate results than the Ranzi scheme. The comprehensive model was positively validated against a broad range of production parameters (pyrolysis temperature: 500°C - 840 °C, diameter of particles: 10 mm - 20 mm, shapes: cylinders and spheres). Investigation showed a pattern in volatiles release profiles and homogeneous heating rate distribution when particle size is below 4 mm. Despite basing the models on the literature's data, the study includes novel and valuable insights for biomass conversion and constitutes a solid foundation for future development.

Keywords

wood, pyrolysis, thermally thick regime, CFD, heat transfer,

Highlights

- Anisotropy is required to model gas velocities in single particle pyrolysis correctly
- The heat sink drying model is generally recommended for moist wood
- The Ranzi-Anca-Couce kinetic scheme shows higher accuracy than the Ranzi scheme
- The developed model has a good accuracy within the broad range of parameters
- Particles smaller than 4 mm can achieve a high heating rate over the whole volume

1. Introduction

Replacement of fossil fuels with biomass in combustion processes as a means of reducing excessive GHG gas emissions has become under severe debate, e.g., in the European Commission [1, 2]. At the same time, the conversion of biomass toward sustainable production of chemicals and carbonaceous materials has become a generally accepted solution for emissions mitigation [3]. Through the years, thermochemical conversion technologies of biomass have been emerging on the market. However, technologies of large-scale production of biofuels and functional materials from biomass are burdened with the high risk related to partially randomized product quality and the inability to tailor the end product. Such a situation is caused by a not complete understanding of the mechanisms occurring during the process, hence a lack of their comprehensive and quantitative description. That hinders the optimisation of process control, assurance of product quality and, in the end, reduction of risks related to the implementation of the technologies on the market.

A purely experimental approach does not solve the problem, mostly due to difficulties in assessing the influence of parameters that critically affect the pathway of conversion, such as heating rate. The solution that may lead to the acceleration of finding the solution is coupling the experimental approach with numerical-based tools like computational fluid dynamics (CFD) modelling. Numerical studies provide an in-depth look into the mechanisms of the process, which is highly difficult to assess experimentally and ease the quantification relationships between parameters. Such a type of study also requires less resources than experimental work [4]. Therefore, at the current stage of development, the conduction of the only experimental study without support from the CFD-based tool may be insufficient to provide novel insights, hence not helpful in finding the answers to the existing problems. However, prior to their use, the numerical tools need to be refined to prevent the transfer of error caused by a model to result, ensuring the reliability of results.

Wood is currently the most applied biomass at large scale thermochemical processing. A significant reduction of the wood's particle size through grinding represents an extensive cost for industrial

processing. Therefore, in conventional processing (e.g., kilns, retorts, auger reactors), wood is applied in the form of chips, chunks, or logs [5, 6]. Conversely, in lab-scale investigations of thermochemical conversion, wood is usually finely ground (below several mm in size). Most wood species have values of thermophysical properties (e.g., density, specific heat) within a similar range, so the particle size becomes the main parameter that dictates which phenomena have a major influence on its conversion, hence the thermal regime [7, 8]. Contrary to finely ground particles, whose conversion is determined mainly by the kinetic regime, so reaction kinetics, large particles in the form of chips or chunks belong to the thermally thick regime, and their conversion is determined by heat transfer [8-11]. It is the most complex scenario where the comprehensive description of the thermochemical conversion process needs to include a reliable description of all phenomena that influence the heat transfer within a single particle of wood.

Single particle models are commonly used CFD-based tools for numerical investigation of the pyrolytic conversion in the thermally thick regime. Besides kinetic changes of the material's constituents, the single particle models also include changes in the particle's structure, thermo-physical properties, and, for the porous materials, the intrinsic gas and vapour flow within the pores [12, 13]. Wood is a porous composite material with anisotropic properties and heterogenous bio-composition. Due to those properties, an appropriate description of the thermochemical conversion of wood in the thermally thick regime is a difficult task. Numerous reviews can be found in the literature about the pyrolysis of single woody particles and its modelling. However, they mostly focus on the assessment of the accuracy of specific models and not on the general impact of the implemented model's components like directional dependency, relationships between parameters and kinetic schemes [7, 8, 14-23]. Nonetheless, those components have a crucial impact on the simulated heat transfer. So far, a comprehensive comparison of the influence of a specific model's component on the heat transfer within a wood particle during pyrolysis has not been made. Therefore, there is no direct guideline of which description of the components should be used to obtain satisfactory model accuracy and reliability.

Structural properties of wood (size of the lumens/vessels and orientation of cell-wall fibres) are a foundation of directional dependency of its parameters (anisotropy). Virgin wood and char have three distinctive directions: longitudinal, radial and tangential. Hence, in each direction, wood and char's thermophysical properties (thermal conductivity, permeability and diffusion coefficient) differ in value. However, an insignificant difference in the parameters along the radial and tangential direction allows for treating them equally, unlike the parameters along the longitudinal direction [24-26]. Spherical particle theoretically has an infinite number of symmetry axes, so in modelling studies, its geometrical representation is often reduced to one dimension [16, 27, 28]. On the other hand, at least two dimensions are required to implement the anisotropic properties, so 1D models always correspond to isotropic properties [20, 29, 30]. Models with more than one dimension have become standard in recent single particle studies [31-34]. Nevertheless, even if the number of dimensions in the model allows for implementing particle's anisotropy, the reported studies often neglect it or implement anisotropy only partially (e.g., only for the thermal conductivity, but not for permeability) [27, 32, 33, 35, 36]. Therefore, basing on the available literature, it cannot be stated how relevant is the implementation of the particle's anisotropy on the outcome of the single particle model of wood pyrolysis.

The moisture content in virgin wood negatively influences the energy efficiency of the pyrolysis process, so a reduction of the moisture content prior to conversion (air-drying, heat-drying) is a common practice [37-40]. When moisture is present within the particle during conversion, strong endothermic water evaporation occurs, severely changing the heat transfer. That, in the end, has non-negligible consequences for conversion in the thermally thick regime [41, 42]. Therefore, an appropriate description of moisture mobility and evaporation is essential for model prediction accuracy [15-17]. In literature, three moisture evaporation models are the most commonly applied: kinetic model, equilibrium model and heat sink model [16, 26, 32], but hybrid approaches also can be found [43]. A recent study on the comparison of different evaporation models' performance suggests that the heat sink model leads to the highest precision in model prediction. However, the investigation

was conducted on a 1D model (isotropic), and its conclusions suggest confirming the observations on higher-dimensional models [16].

The reaction kinetics applied to the model have a multifaceted influence on simulated heat transport within the particle due to its connection to reaction heat and the change in thermo-physical parameters of components. One of the first kinetic schemes of wood thermal degradation is the one proposed by Safizadeh and Chin [44]. Along with the requirement for higher model accuracy, it has been modified and extended, e.g. by adding intermediate stages [27]. Nonetheless, such improvements are limited since they do not account for detailed chemical changes of components. The precise description of degradation reaction kinetics for each bio-constituent is a task that has not yet been achieved due to the complex nature of the problem [20]. However, the lumped kinetic scheme proposed by Ranzi et al. [45, 46], which covers the parallel degradation of each bio-polymer and the formation of the most abundant products, provides an elegant partial solution to that issue. The Ranzi scheme was founded on TGA-based experimental work so the conversion of small biomass particles. Therefore, the Ranzi scheme is the most applicable for the pyrolysis of small particles (kinetic regime), but for the conversion of particles in the thermally thick regime, its predictions are also accurate [31, 32]. Size of the particle pose a non-negligible limitation in the heat and mass transfer, which leads to restrictions in the evaporation of e.g., carbohydrates derivatives. It translates into changes in the degradation pathway of wood components, hence elevated formation of lighter compounds and char and changes in reaction heats [47-51]. Anca-Couce et al. proposed an extension of the Ranzi scheme to account for the limitation caused by the particle size [52, 53]. The limitation is reflected by the parametrically controlled conversion path called “secondary charring”, which is incorporated into the lumped kinetic scheme (Ranzi-Anca-Couce, RAC scheme). Due to a lack of the reliable correlation between the extent of secondary charring and the conversion parameters (e.g., heating rate, particle size), for now, the extent of the secondary charring has to be subjectively estimated for modelled case. Despite the aforementioned flaw, the RAC scheme has been positively validated with data from the wood pyrolysis in the thermally thick regime and also show a good

prediction accutracy [28, 54]. A direct comparison of both detailed kinetic schemes (Ranzi and RAC) does not yet exist in literature. Therefore, questions arise on how differences in the schemes affect the outcome (profiles of temperature, mass loss and vapours release and heat of reactions) and, more importantly, which ones can be selected as being more appropriate to implement.

Experimental and numerical investigations on the pyrolysis of a single wooden particle concerning the pyrolysis temperature have been amply described in the literature, but only a few focused on particle size [27, 31, 33, 54-57]. Among those, only the experimental study of Attaya et al. investigated the relationship between three parameters: pyrolysis temperature, particle size and shape [33]. In the latter study, the broad experimental data was used to validate the single particle model proposed by Park et al. (simple kinetic scheme and isotropic permeability) [27]. In view of finding the solution to the quantitative relation between process and product parameters, the reproduction of the already published data for model construction or validation purposes will not bring novel insights. Therefore, considering the abundant experimental data available in the literature, which theoretically should not be biased or inaccurate, it seems advisable to use the published experimental data as a foundation for the CFD comprehensive model. That is especially attractive since the advanced models with complete anisotropy of particle, combined with detailed kinetic schemes of bio-components degradation, have not been validated with most experimental datasets. With such an approach, each part of the model can be validated on a separate dataset, leading to the construction of a comprehensive model able to simulate various processes in a broad range of conditions with appropriate accuracy and reliability. Then such a model could be used for objective investigation of the relationships of process parameters to the heating rate distribution.

This study aimed to provide an unbiased and state-of-the-art comprehensive model to investigate the distribution of the heating rate within the single wood particle during pyrolysis in broad process conditions. The study starts from a stepwise development of a model to ensure that each model's component description results in the highest possible reliability and accuracy from available solutions.

In this study, the commonly used practice of calibration of model parameters was not applied to fit the experimental data. Instead, the chemical and thermophysical properties of wood for each step model were selected meticulously and with to highest possible accordance with the real properties of the woods of the experimental research (directly taken from the work or matched to the wood species from the literature [18]). Then, into the step model, the different descriptions of the investigated phenomena was implemented, and their result was compared to find the best possible description. After a few steps of development, the comprehensive model was validated over a broad range of process parameters and then used for the investigation of the heating rate distribution. The study also includes a critical discussion on each step of the development as well as the extensive elaboration of the pathway that can lead to the further development of the area of biomass pyrolysis in a thermally thick regime.

This manuscript is divided into four parts, each devoted to a specific issue:

1) Part 1: The relevance of implementing wood anisotropy into the model and the accuracy of several drying models (kinetic, equilibrium and heat sink model). The validation was based on the experimental pyrolysis at 900 °C of cylindrical wood particles with an initial moisture content of 6 wt. % and 40 wt. %, made by Lu et al. [43].

2) Part 2: The accuracy of different kinetic schemes (1 simple: Safizadeh and Chin, and 2 detailed: Ranzi and RAC) in the prediction of temperature profiles, specific compound release profiles, and yields of lumped products. The model validation is based on the experimental pyrolysis of cylindrical, dry wood particles at 418 °C made by Benandji et al. [55].

3) Part 3: The accuracy in predicting temperature and mass loss over a broad range of pyrolysis temperatures, particle sizes and shapes. Then on the validated, comprehensive model, the effect of process conditions on heating rate distribution. Validation is based on previously established experimental results from pyrolysis of particles with 2 shapes (spherical and cylindrical), each in 3 different sizes, pyrolysed at 4 different temperatures (ranging between 500 °C and 840 °C) made by

Attaya et al. [33]. Despite spherical particles not being representative for industrial-scale processing [6, 19], such a shape is widely used in models with a dimensional reduction to 1D, so it was retained.

4) Part 4: Overview of the performance issues of models in view of the relation between implemented model components and heat transfer. This section provides suggestions for model developmental pathways for pyrolysis of single, large wooden particles.

2. Numerical setup

2.1. Model foundation

All modelled geometries were built as porous media according to the description provided by Grønli [26], which had already been validated in other studies [15, 16]. Depending on the scenario, maximally, four phases were distinguished: solid, bound water, liquid water and gas. To obtain optimal computational efficiency and to remove the phenomena and correlations whose relevance is not essential, and which simultaneously are very burdening, the following assumptions were applied for all models:

1) The description of fluid dynamics was simplified from Darcy and Forchheimer's to a pure Darcy's description. That assumption was made based on two criteria [58]: Reynolds number << 10 and Forchheimer number << 0.11, which both were fulfilled for the investigated scenarios. Calculation of the Reynolds number and Forchheimer number for an exemplary case is provided in the Supplementary Information in Section S4.

2) Intrinsic transport of mass within the domain occurs by convection and diffusion. The diffusion of all compounds is temperature-dependent and modelled according to Fick's binary diffusion law. The mass boundary condition is modelled as a convective mass transfer.

3) Due to a sufficiently large Péclet number for heat transfer, thermal equilibrium between all existing phases is assumed on a given location with the modelled particle domain. The enthalpy for all phases is a linear function of temperature. The gas phase is considered as an ideal gas.

4) Internal heat transfer occurs by conduction, convection and radiation and the thermal boundary condition is described by radiative and convective heat transfer.

5) The model geometry only covers the particle, and the surrounding environment is not included. Therefore, secondary gas-phase reactions (e.g., thermal cracking of volatiles, gasification and water gas shift reactions) are not implemented into the model. Vapour recondensation was assumed to be not relevant, so it was omitted [16].

6) Values of thermo-physical parameters and bio-chemical composition of wood and char used in a specific model (if measured) were used directly from the experimental work or (if not measured or disclosed) matched as close as possible to the wood species from the literature [18]. Within each investigated scenario, models differ with the description of the specific component but not with the parameters.

7) In the models, only 3 base wood constituents are distinguished: cellulose, hemicellulose and lignin, which, if needed, were normalised to 100%. Other components (ash, extractives) are neglected due to the assumption of their low concentration in the investigated cases, which for instance for the case of stem wood are typically below 5 wt. % [59, 60].

8) For simplicity and comparability within every scenario, the conversion products were lumped into product groups: bio-oil (light and heavy condensable compounds and water), pyrolysis gas (non-condensable compounds) and char (char + metaphase). The moisture content (MC) wt. % is defined as the mass of moisture per total mass of matter (water + biomass). The wt. % for the mass of the pyrolysis products refers to the mass of specific or lumped product per initial mass of dry biomass.

9) Thermo-physical properties of solids are modelled as linearly dependent on the degree of conversion. The enthalpy for all phases is a function of temperature.

10) The effective specific heat for the solid and gas phase is calculated from the share of the specific heats of the lumped product groups (biomass, char, heavy condensables, light condensables, water vapour, permanent gases), and not based on the concentration of the individual, specific compound.

11) In the applied software (COMSOL^{TM}, version 5.5), it was not possible to implement the shrinking of the geometry (as drying and pyrolysis proceed) in a reliable manner. Therefore, despite that the mechanical changes in the particle may have a significant influence on particle conversion, shrinkage, cracking, and fragmentation of the domain during drying and pyrolysis were omitted [61-63]. Details about the issue can be found in Section S5 in the Supplementary Information.

12) Due to large computational requirements, the computation of models from Part 3. (Section 3.3) was conducted in parallel mode using the HPC (High Performance Computing) infrastructure located at Ghent University.

The Supplementary Information (Section S1, S2) provides detailed information regarding: fundamental, governing and auxiliary equations, and boundary conditions. The parameters that are not changing between models are listed in Table S2, and the parameters corresponding to a model in a specific scenario are provided in the related Section. In each Part of the study, only one description varied between scenarios, while all other parameters and descriptions of the sub-models remained constant. Also, when adjustment was implemented, the parameter or description was adjusted for all scenarios to assure the highest objectivity of the investigation.

Due to the assumption of similarity between the tangential and radial direction in a wood particle, the models did not require to distinguish 3 dimensions to implement anisotropy. Therefore, the use of 2D-axisymmetric domains in the models was preferred, considering that the shape of a particle in every

investigated scenario had a symmetry axis (cylinder or sphere). In Section S3 of Supplementary Information, additional information on the hardware used for the study (Section S3.1), the configuration of the solver, simulation convergence (Section S3.2) and selection of the meshes and maximal time step for each part of the study (Section S3.3) has been provided.

2.2. Directional dependence of wood thermophysical parameters

Wood is an anisotropic (orthotropic) solid, so parameters dependent on the fibre and vessel orientation are implemented as an isometric tensor, defined as:

$$\Lambda = \begin{bmatrix} \Lambda_{r,r} & 0 & 0 \\ 0 & \Lambda_{\varphi,\varphi} & 0 \\ 0 & 0 & \Lambda_{z,z} \end{bmatrix} \quad (1)$$

Where $\Lambda \in \left[K_{ph,in}, \lambda_S\right]$, $K_{ph,in}$ is the intrinsic permeability of a phase (gas or liquid water), λ_S is the effective thermal conductivity of a solid, and the subscript denotes the direction of the parameter in a cylindrical coordinate system. In the models, the assumed parameter values in the tangential and radial direction are insignificantly different, so the tensor is reduced to 2 directions (longitudinal and radial). According to Thurman and Lecker [64], the transformation from anisotropy into isotropy can be done by averaging the parameter values with an equal share of each direction (1/3 longitudinal + 1/3 radial + 1/3 tangential). However, Park at al. [27] have shown that the transformation correlation proposed by Ozisik [65] is more accurate than Thurman and Lecker's [64], so in the models, the correlation for the transformation from anisotropy to isotropy was implemented as:

$$\Lambda_{ISO} = (\Lambda_{r,r} \cdot \Lambda_{\varphi,\varphi} \cdot \Lambda_{z,z})^{1/3} \quad (2)$$

Where Λ_{ISO} is the value of the direction dependent parameter transformed into the isotropic average.

2.3. Drying models

2.3.1. Kinetic (KIN)

The kinetic drying model assumes a first-order Arrhenius reaction of water (bound or liquid) conversion into vapour:

$$\dot{\omega}_{e,KIN} = k_{e,KIN}(< \rho_L > + < \rho_B >) \quad (3)$$

Where $\dot{\omega}_e$ [kg/(m^3·s)] is the evaporation rate, $k_{e,KIN}$ [1/s] is the evaporation rate of the kinetic drying model, $< \rho >$ [kg/m^3] is the bulk density, and the subscript L and B denote liquid and bound water, respectively. Prior to the implementation, a pre-assessment of the most accurate kinetic model was performed. The details of the drying model selection are presented in Supplementary Information, Section S6.1. In relation to the conducted pre-selection, the kinetic parameters A_{KIN} = T [1/s] (where T is the temperature in Kelvin) and $E_{a,KIN}$ = 33 [kJ/mol] from Gentile et al. were selected as leading to the most accurate results, so they were applied in the model in Part 1 [32].

2.3.2. Heat sink model (HS)

The heat sink model (thermal drying model, heat flux model) assumes that water evaporation in a representative volume occurs only at the boiling temperature, and the temperature stays constant until all water is evaporated [16, 43, 66]. According to Haberle et al. [16], it is described as:

$$\dot{\omega}_{e,HS} = \begin{cases} f_{evap}\,\dfrac{j_{Heat}}{H_e} & if\ \ T \geq T_e\ and < \rho_L > > 0 \\ 0 & otherwise \end{cases} \quad (4)$$

Where T_e is the water boiling temperature, set on a fixed value of 100 °C, H_e is the latent heat of water evaporation (set on a fixed value 2440 kJ/kg [16, 43]), j_{Heat} [W/m^3] is the heat flux towards the representative volume and f_{evap} [-] is an unitless, evaporation fraction factor. The value was set at a fixed value 0.80, in relation to a conducted sensitivity analysis. The details of this preliminary sensitivity

analysis can be found in the Supplementary information Section S6.2. With the assumption that heat transferred with the movement of water is negligible, the heat flux towards the representative volume is defined as:

$$j_{Heat} = \nabla(\varepsilon_G u_G < \rho_G >^G C_{p,G} - \lambda_{eff} \nabla T) \quad (5)$$

2.3.3. Equilibrium model (EQ)

The equilibrium model assumes that an equilibrium between liquid water and water vapour exists at any time inside the particle's pores, and the water vapour's partial pressure at any given time tends to be equal to the saturation vapour pressure. Therefore, it can be stated that:

$$< P_v^{eq} >^G = \begin{cases} P_{sat} & if\ MC > MC_{FSP} \\ P_{sat} \cdot \kappa(MC_B, T) & if\ MC \leq MC_{FSP} \end{cases} \quad (6)$$

Where MC [-] is the moisture content on a mass basis, MC_{FSP} [-] is the moisture content at fibre saturation point, $< P_v^{eq} >^G$[bar] is the equilibrium's partial pressure of water vapour, P_{sat} [bar] is the saturation vapour pressure, $\kappa(MC_B, T)$ [-] is the relative humidity factor. The saturation vapour pressure was implemented as [67]:

$$P_{sat} = \exp\left(24.21 - \frac{467.35}{T}\right) \quad (7)$$

The equation for the wood's relative humidity factor was calculated from [26]:

$$\kappa(MC_B, T) = 1 - \left(1 - \frac{MC_B}{MC_{FSP}}\right)^{6.453 \cdot 10^{-3}\, T} \quad (8)$$

From the equilibrium partial vapour pressure, the vapour density was obtained through the equation:

$$< \rho_v^{eq} >^G = \frac{< P_v^{eq} >^G M_{H_2O}}{RT} \quad (9)$$

Where M_{H_2O} [kmol/kg] is the molecular mass of water. The final equation for the water evaporation rate is defined as:

$$\dot{\omega}_{e,EQ} = \frac{\varepsilon_G(< \rho_v^{eq} >^G - < \rho_v >^G)}{t_{eq}} \quad (10)$$

Where $< \rho_v^{eq} >^G$ [kg/m^3] is the equilibrium vapour density, $< \rho_v >^G$ [kg/m^3] is the water vapour density at a given time and t_{eq} [s] is the time required to reach equilibrium between the vapour density and theoretically assumed saturation vapour density ("equilibration time"), which was set at a fixed value of 10^{-3} s [15].

2.4. Kinetic schemes of primary biomass degradation

2.4.1. Single component competitive scheme (Simple)

The single-component competitive scheme of biomass pyrolysis, besides mass loss, aims to predict the yield of the three main products (char, bio-oil, and gas) without their detailed composition. In this study, the kinetic scheme proposed by Shafizadeh and Chin [44] with kinetic parameters from Thurner and Mann [68] has been applied as the single component competitive scheme. The scheme and its parameters are provided in Table S4.

2.4.2. Ranzi kinetic scheme (Ranzi)

The Ranzi model combines all findings related to the thermal decomposition of each major component of biomass [69-71]. The scheme distinguishes cellulose, hemicellulose (2 types), and lignin divided into 3 artificial types of lignin: LIG-H, LIG-O, and LIG-C (hydrogen-, oxygen- and carbon-rich, respectively) [72-74]. Additionally, the carbonaceous residue is defined as the char (the elemental carbon, C) and the volatiles "trapped" within the char's metaplastic phase, called here char's metaphase (G[X]). The metaphase represents the trapped volatiles that can still undergo release, e.g., through carbon matrix

reorganisation or conversion in a “trap”. The kinetics of metaphase change should mimic its formation from bio-components and subsequent degradation, so the devolatilisation of the char. The Ranzi model has evolved since its introduction [31, 32, 45, 75-77], and it currently covers 25 reactions and involves 48 compounds. In this study, not all reactions and compounds were implemented (since the extractives content was neglected). Table S5 summarizes the Ranzi scheme, and its parameters used in this study [32, 77].

2.4.3. Ranzi-Anca-Couce scheme (RAC)

The RAC scheme is a modification of the Ranzi scheme [52, 78], and it currently contains 24 reactions, 33 compounds and 4 adjustable parameters [53, 54]. The adjustable parameter “x” defines the share of the alternative degradation (secondary charring) route in the overall process. The extent of secondary charring is assigned separately for each bio-component: cellulose (x_{CELL}), hemicellulose (x_{HCE}), lignin (x_{LIG}) and metaphase ($x_{G[X]}$). Due to a lack of correlation between process conditions and the extent of secondary charring reactions, the values of these parameters have to be selected subjectively before the simulation in each model. Table S6 provides the RAC kinetic scheme and corresponding parameters used in this study [53, 54].

3. Results and discussion

3.1. Relevance of implementation of wood anisotropy and influence of a specific drying model

3.1.1. Model foundation

In this Section, the results from the models from Part 1 are presented, which cover the investigation of the influence of directional dependency of wood properties and the performance of specific drying models. The specific parameters of the modelled wood cylinder, based on the work of Lu et al. [43] and used in the models of Part 1 are shown in Table 1. Values of the poplar wood's thermal conductivity

were selected from the literature [79, 80], as they were not experimentally measured in the referenced study. For the same reason, the gas permeability in wood was obtained from Comstock [24]. However, there was no data in the literature regarding gas permeability in char derived from poplar wood. Therefore, the gas permeability of poplar char was selected subjectively, taking into consideration the wood anisotropy and correlations in gas permeability between wood and char, which are known for other wood species [18]. The kinetic scheme based on Shafizadeh and Chin (Table S4) was used in the model.

Table 1. Specific parameters of the Part 1 models in accordance with the work of Lu et al. [43] (longitudinal direction on the z-axis and radial direction on the r-axis).

Parameter	Symbol	Unit	Value
Particle	*Cylinder, moist poplar wood*		
Diameter	D	[mm]	9.5
Height	H	[mm]	38.0
Moisture content	MC	[wt. %]	6 / 40
Bulk density (dry)	$< \rho_S >$	[kg/m^3]	580
Thermal conductivity			
Biomass (Longitudinal)	$\lambda_{Biomass,z}$	[W/(m·K)]	0.315
Biomass (Radial)	$\lambda_{Biomass,r}$	[W/(m·K)]	0.150
Char (Longitudinal)	$\lambda_{Char,z}$	[W/(m·K)]	0.215
Char (Radial)	$\lambda_{Char,r}$	[W/(m·K)]	0.100
Permeability			
Biomass (Longitudinal)	$K_{Biomass,z}$	[m^2]	$1 \cdot 10^{-14}$
Biomass (Radial)	$K_{Biomass,r}$	[m^2]	$5 \cdot 10^{-16}$
Char (Longitudinal)	$K_{Char,z}$	[m^2]	$5 \cdot 10^{-13}$
Char (Radial)	$K_{Char,r}$	[m^2]	$1 \cdot 10^{-13}$
Boundary temperature			
Gas	T_{Gas}	[°C]	780
Wall	T_{Wall}	[°C]	960
Initial	T_{Ini}	[°C]	25

For models assessing the influence of anisotropy, the thermal conductivity and permeability were implemented according to eq. (1), and for the isotropic scenario, the parameters have been calculated according to eq. (2). Additionally, in the latter models used to investigate the influence of anisotropy, the kinetic (KIN) drying model was implemented. In the models used for assessing the influence of the selected drying model, the following three different drying models were implemented: (kinetic (KIN), equilibrium (EQ) and heat sink (HS) models) and were compared. Also, in compared the different drying models, the anisotropic properties in the latter models of wood were implemented.

3.1.2. Influence of the directional dependency of wood properties

Implementing the directional dependence of the thermal conductivity in the wood had a noticeable influence on the simulated temperature profiles (at the centre and the base's surface) and mass loss (fig. 1). Details of the relation between the reaction heat and the temperature profile are provided in Section 3.2. As observed through the simulated centre temperature profiles, in the isotropic model, the moisture is released quicker than in the anisotropic model, for both initial moisture contents. Despite the noticeable difference in the centre temperature profile between both models, it is not severe. The mass loss profiles show only a marginal difference between anisotropic and isotropic models. Therefore, considering possible measurement error (and uncertainty) of the experimental results, the objective indication about which description leads to more accurate results in terms of temperature and mass loss prediction remains inconclusive.

The isotropic description lowers the thermal conductivity in the longitudinal direction, which leads to its higher thermal resistivity. Such a change leads to higher heat accumulation in the region closer to the particle boundary, so less energy is transported toward the centre. In turn, this is assumed to be the cause of the more rapid temperature increase at the particle base's surface for the isotropic model compared to the anisotropic model. However, a more complex surface temperature profile can be observed for the anisotropic model, especially close to the end of conversion (fig. 1, Top and Middle),

which is caused by a fluctuation of the heating rate. That suggests the presence of a factor other than thermal conductivity, which influences the heating rate at the particle's base surface in the models with implemented anisotropic properties of wood.

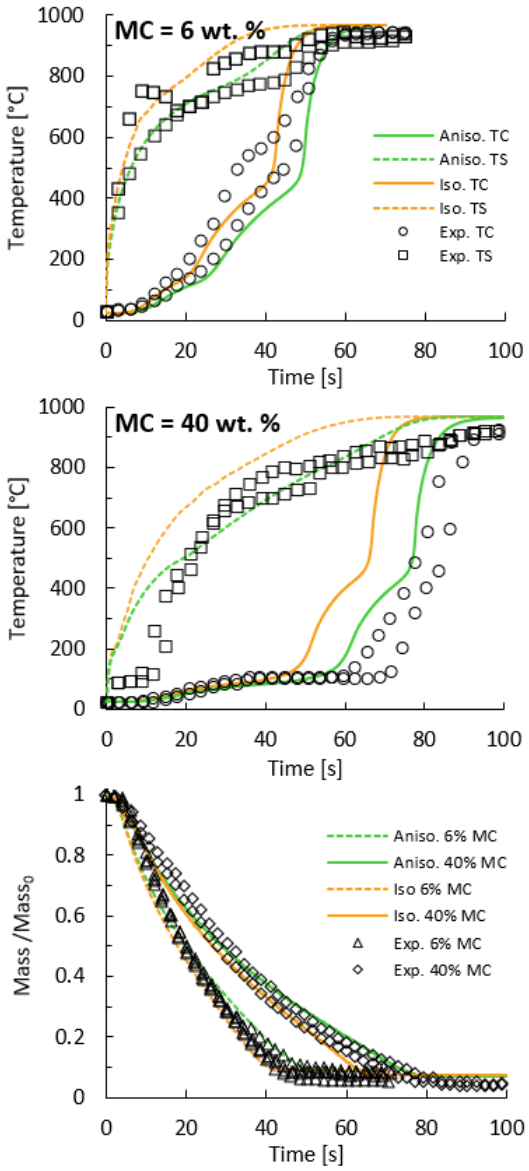

Fig. 1. Simulated profiles of centre temperature (TC), base surface temperature (TS) and mass loss (ML) from isotropic (Iso.) and anisotropic models (Aniso.) with the experimental data (Exp.) from Lu et al. [43] (Top - TC and TS for6 wt. % MC, Middle - TC and TS for 40 wt. % MC and Bottom - ML for both MC).

The gas permeability (related to pressure drop per distance) and the length of the pathway from the point of gas production to its release from the particle (surface) dictate the strength of the restriction to gas flow. The gases always choose the path of least resistance, so if the difference in the pathway length is less substantial than the difference in gas permeability, the gas will choose the release pathway with a higher gas permeability. In models with the anisotropic description, the gas permeability is significantly higher in the longitudinal than in the radial direction, so the influence of permeability is much more relevant in terms of gas release than the difference in pathway length between directions. Therefore, in anisotropic models, the escape path of evolved pyrolysis vapours is predominantly longitudinally-oriented (fig. 2). Several modelling studies initially indicated the existence of such behaviour of gas and vapours during wood pyrolysis [13, 22, 81-83]. Then, such phenomena were confirmed experimentally by Brackmann et al. [29] and investigated with a model based on a detailed wood structure by Ciesielski et al. [20]. In the isotropic model, the pressure drop per distance is the same in every direction, so gases travel through the shortest possible escape path. Hence their escape path is radially oriented and not longitudinally (fig. 2). A similar outcome was obtained in numerical studies on models in which isotropic gas permeability was assumed [32, 35].

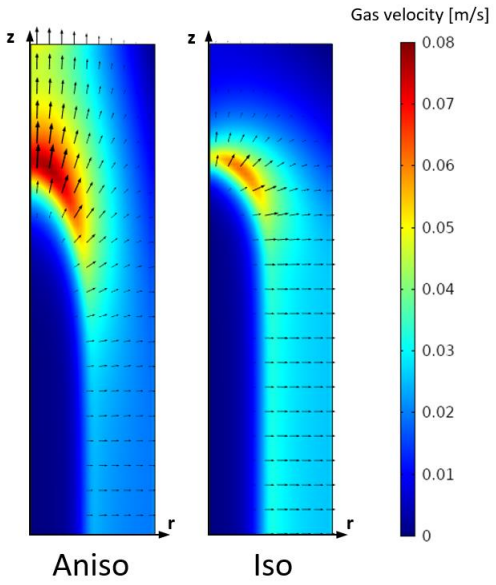

Fig. 2. Simulated distribution of the intrinsic gas velocity at 70% conversion for MC = 40 wt. % and anisotropic (left) and isotropic (right) gas permeability.

The escape path of the evolved vapours leads through the already converted char zone, which has a higher temperature than the initially evolved vapours [84, 85]. Therefore, with the assumption of thermal equilibrium between phases, the vapours convectively transported through the hot char zone will absorb heat, leading to a cooling effect of the solid char [13, 81, 85]. This cooling effect causes a reduction in the heating rate in the zone through which the gases escape. In the end, this cooling effect is recognised as a factor influencing particle conversion [13]. The cooling effect's intensity depends on the amount of vapours evolved during conversion, so an elevated initial moisture content in wood through the creation of excess of water vapour enhances this cooling phenomenon [42]. The cooling effect is the factor that changes the shape of the temperature profile at the particle's base surface in the anisotropic model when compared to the isotropic model (fig. 1). Moreover, assuming a permeability independent of direction (isotropy) leads to the prediction of an inappropriate gas velocity distribution within the particle (fig. 2). That translates to a lack of convective cooling in the direction of higher gas permeability. Despite the inconclusive relevant effect of the directional dependency of the thermal conductivity for the investigated particle, the anisotropy of the gas permeability is required to predict the behaviour of a single wood particle during pyrolysis in an accurate manner. Not implementing the directional dependency of the gas permeability can also be a factor contributing to an inappropriate simulated composition and release profile of vapours in case if the consecutive reactions in the vapour-phase are implemented into the model (e.g., cracking of heavy condensables). Additionally, it is suspected that the inconclusive difference in the simulated centre temperature profile between the anisotropic and isotropic model, so differences in the thermal conductivity, are related to the relatively small size of the modelled particle. Consequently, the results would be more unambiguous for larger particles (e.g., chunks) [17, 86]. Overall, it is advised to implement the anisotropic description of the parameters into a model of pyrolysis of a single wood particle (if possible), because then the behaviour of a wood particle is simulated in a more realistic, hence more reliable manner. The anisotropic description may not be critically needed for implementation when the particles are converted in the kinetic regime (fine powders) because then

the internal heat transfer does not play a major role. On the other hand, the anisotropy seems to be very relevant for all other regimes (thermally thin regime, thermal wave regime, and thermally thick regime like in this study). Nonetheless, such a statement must be confirmed by appropriate investigation to obtain an objective meaning and identify the threshold sizes.

3.1.3. Accuracy of common drying models

The second element of the Part 1 investigation was assessing the performance of different, commonly applied descriptions of moisture evaporation during pyrolysis of a single wood particle. As shown in fig. 3, among all investigated drying models, the equilibrium model (EQ) noticeably overpredicted the temperature of water evaporation (i.e., boiling point) at the particle centre for both initial moisture contents. For a particle with 6 wt. % initial moisture content, the kinetic (KIN) and heat sink (HS) model results are highly comparable. However, for a particle with an initial moisture content of 40 wt. %, the difference between the models becomes more visible. In the higher initial moisture content scenario, the KIN model slightly underestimates the temperature of water evaporation at the particle centre. That, leads to a difference in the simulated heating rates by reducing the heat required to bring the water to its boiling point. In the end, this is visible as a quicker water release in the KIN model in comparison to the HS model. As can be observed, the selection of appropriate wood properties and the drying model parameters leads to a very similar temperature profile of the base and centre of the modelled particle.

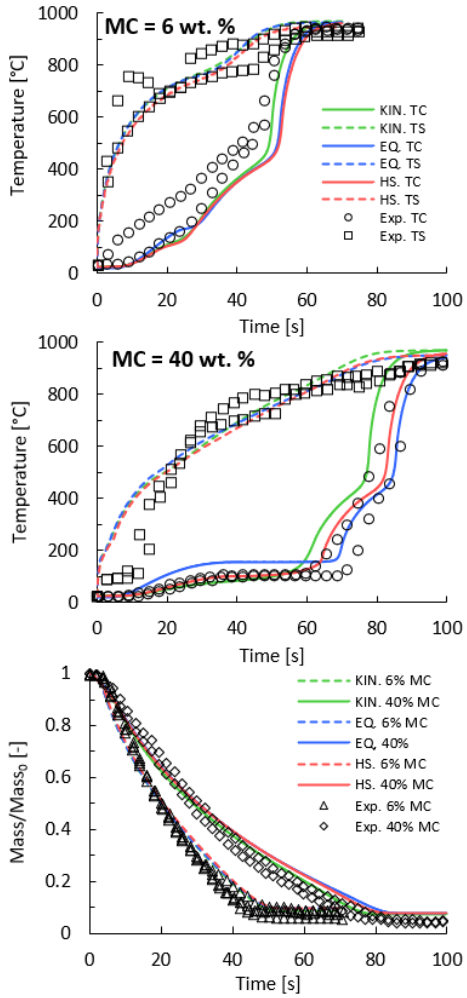

Fig. 3. Comparison of simulated profiles of centre temperature (TC), base surface temperature (TS) and mass loss (ML) from different drying sub-models: kinetic (KIN), equilibrium (EQ) and heat sink (HS) model with the experimental data (Exp.) from Lu et al. [43] (Top - TC and TS for 6 wt. % MC, Middle - TC and TC for 40 wt. % MC, and Bottom - ML for both MC).

The simulated mass loss profiles from all drying models were also very similar and presented a good fit to the experimental data (fig. 3, Bottom). As expected, the mass loss profile from the KIN model in the 40 wt. % initial MC scenario showed a slightly faster mass loss in comparison to the other drying models. The latter is related to the lower water boiling point simulated by the model and elevated evaporation rate, which caused the prediction of a faster conversion due to lower heat requirement. Despite the similarity in mass loss profile, the final char yield was predicted to be different according to the drying model used (fig. 4). The simulated char yield with the KIN model for both initial moisture

contents was lower than for the other investigated drying models, although, in simulations with the EQ and HS model, yields were comparable. For every drying model, a higher initial MC led to an increase in the predicted char yield, which is in agreement with other experimental and numerical works [41, 42]. The influence of the initial MC on the char formation is depicted in the simulated char yield distributions (fig. S5). The higher initial MC increases the evaporative heat absorption along with convective cooling, which leads to a reduction of the heating rate. In the Shafizadeh and Chin kinetic scheme applied in this model, the predicted mass ratio of bio-oil to char at 350 °C is 30, but at 550 °C, this ratio almost doubled. Therefore, in the simulation with a high initial MC (and thus lower heating rate), the conversion occurs at lower temperatures, which is favourable for char formation. For low initial MC, the rapid increase in temperature shifts the conversion in favour of bio-oil and pyrolysis gas formation.

Despite the predicted trend of MC on char yield being in agreement with other literature works [41, 87], the trend in the simulated char yield does not match the absolute values nor the trend seen in the employed experimental validation data, where the char yield decreases with the initial MC. In the study by Lu et al., pyrolysis of a moist wood particle was performed at a temperature of ca. 1000 °C [43]. Therefore, phenomena other than bio-components degradation, which were not implemented in the models, may become significant (e.g., the Boudouard reaction above 710 °C [88], and steam gasification above 600 °C [89-91]). The influence of steam gasification in relation to moisture content is also suggested by the simulated water vapour distribution within the particles (fig. S6). However, considering the short residence time of water vapour within the particle (less than 60 s for 40% initial moisture content), the significance of such a phenomenon on elevated mass loss is questionable. Additionally, in view of other single particle studies, such a low char yield for higher initial moisture content seems unrealistic [30, 33, 54]. Therefore, it is suspected that the experimental char yield may be burdened with error, and it may be the main cause of the deviation of the trend as predicted by the models in this study and the experimental results from Lu et al. [43].

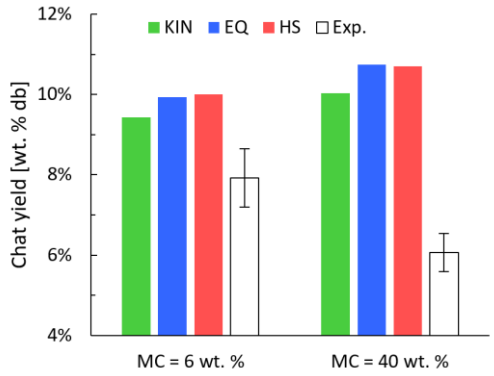

Fig. 4. Simulated char yields (db.) with MC = 6 wt. % and 40 wt. % using KIN - kinetic, EQ - equilibrium and HS - Heat sink drying sub-models, and experimental data (Exp.) from Lu et al. [43].

The outcome of this study is very similar to the results obtained by Haberle et al. [16]. The deviation between studies in the temperature profiles obtained with the KIN model is related to the implementation of different kinetic parameters of drying. The KIN and HS model depends only on the intrinsic heat transfer, in opposition to the EQ model, which depends on heat transfer and the mass transfer and fluid dynamics of water vapour. The description of the gas permeability in the EQ model (directional dependency and parameters values) severely influences its performance [15]. The difference in the gas permeability values is assumed to be a major factor leading to deviating results between this study and those obtained by Haberle et al. [16]. The value of permeability was not experimentally measured in the study of Lu et al. [43], so the values of intrinsic permeability in both simulation studies had to be selected from the literature. That may be a cause of the elevated boiling temperature with the use of the EQ model. It is suspected that the selection of more appropriate (real) gas permeabilities could reduce the EQ model's boiling temperature. Due to the experimental uncertainty and small difference in the simulated profiles, it cannot be objectively indicated which model (HS or KIN) gives more accurate results. In both cases, the model does not reflect the physical phenomena, where KIN describes it via the Arrhenius equation (chemical process description), and the HS model includes the evaporation factor. On a purely numerical basis, the HS had the best performance in the investigated study.

The EQ model is the most realistic model, but as shown in this study in may lead to suboptimal results in comparison to the less realistic drying models. The implementation of the EQ model requires very accurate values of the wood properties (especially permeability, which is extremely rarely measured). Otherwise, the results are not precise and may become not reliable. Therefore, unless the modelled particle is well characterised (thermal conductivity and permeability), it is advised to use the HS or KIN drying model. Nonetheless, it needs to be highlighted that in this study, the most suitable kinetic parameters of drying have been selected. As shown in Section S6.1, the selection of the sub-optimal kinetic parameters will lead to very imprecise results for the KIN model. On the other hand, for the HS model, certain accuracy is maintained, even for sub-optimal values of the evaporation factor, whose value is between 0 and 1 (Section S6.2). Therefore, the HS model's use will always be burdened with less risk of inaccuracy within the model, and the adjustment of this drying model is much less complicated than in the KIN model.

3.2. Kinetic scheme and model accuracy

3.2.1. Foundations of the model

This section presents results from models from Part 2, which includes the investigation of the differences in simulation outcomes resulting from the implemented kinetic scheme. The models were based on the experimental work of Bennadji et al. [55] because in the latter study, the employed pyrolysis temperature allows omitting the secondary gas-phase reactions (depending on the literature source, secondary gas-phase reactions are irrelevant in pyrolysis below 500 °C or 650 °C [31, 92]). Moreover, besides temperature profiles and the yields of lumped products, the selected reference study contains the release profiles of several vapour phase compounds, which were used to validate the detailed kinetic schemes. The specific model parameters of the wood cylinder, based on the work of Bennadji et al. [55], used in models of Part 2 are shown in Table 2.

Table 2. Specific parameters of Part 2 models in accordance with the work of Bennadji et al. [55] (longitudinal direction on the z-axis and the radial direction on the r-axis).

Parameter	Symbol	Unit	Value
Particle	Cylinder, dry poplar wood		
Diameter	D	[mm]	19.05
Height	H	[mm]	40.00
Moisture content	MC	[wt. %]	0
Bulk density (dry)	$< \rho_S >$	[kg/m^3]	500
Bio-components conc.			
Cellulose (CELL)	c_{CELL}	[wt. %]	50.50
Hemicellulose (HCE)	c_{HCE}	[wt. %]	29.55
H-rich lignin (LIG-H)	c_{LIGH}	[wt. %]	2.59
O-rich lignin (LIG-O)	c_{LIGO}	[wt. %]	7.38
C-rich lignin (LIG-C)	c_{LIGC}	[wt. %]	9.98
Secondary charring param.			
Cellulose	x_{CELL}	[-]	0.20
Hemicellulose	x_{HCE}	[-]	0.25
Lignin	x_{LIG}	[-]	0.35
Metaphase	$x_{G[X]}$	[-]	0.40
Thermal conductivity			
Biomass (Longitudinal)	$\lambda_{Biomass,z}$	[W/(m·K)]	0.255
Biomass (Radial)	$\lambda_{Biomass,r}$	[W/(m·K)]	0.125
Char (Longitudinal)	$\lambda_{Char,z}$	[W/(m·K)]	0.105
Char (Radial)	$\lambda_{Char,r}$	[W/(m·K)]	0.071
Permeability			
Biomass (Longitudinal)	$K_{Biomass,z}$	[m^2]	$1 \cdot 10^{-14}$
Biomass (Radial)	$K_{Biomass,r}$	[m^2]	$1 \cdot 10^{-16}$
Char (Longitudinal)	$K_{Char,z}$	[m^2]	$5 \cdot 10^{-13}$
Char (Radial)	$K_{Char,r}$	[m^2]	$5 \cdot 10^{-14}$
Boundary temperature			
Gas	T_{Gas}	[°C]	418
Wall	T_{Wall}	[°C]	418
Initial	T_{Ini}	[°C]	95

Similar to Part 1 (Section 3.1), some thermophysical parameters of wood were not measured in the referenced study [55], so their values had to be selected from the literature. The initial wood density was selected from Cobretta et al. [31] and wood thermal conductivity from Lee et al. [93]. However, the thermal conductivity of wood in the radial direction was selected to be higher by 20% than the value obtained from the sourced study, with the presumption that such change is in agreement with

the literature [31, 67, 79, 80]. Gas permeability in wood was selected from Comstock [22], and gas permeability in char, as in Section 3.1.1., was selected subjectively, taking into consideration the change in gas permeability between wood and char, which are known for certain wood types other than poplar [18]. The initial concentration of the lignins [55] (H-rich, O-rich and C-rich lignin) needed for the detailed kinetic schemes was calculated with split parameters, according to Cobretta et al. [31]. In the experiments, wooden cylinders were dried prior to pyrolysis, so the moisture content was neglected, and there was no need to implement a drying sub-model into the particle pyrolysis model.

In Part 2 three scenarios were investigated, each with a different kinetic scheme being implemented into the model: the simple kinetic scheme (Table S4), the Ranzi (Table S5) and RAC (Table S6) kinetic schemes. The simple kinetic scheme was based on the work of Shafizadeh and Chen, without any alteration [44]. The Ranzi scheme was used in its most recent adaptation by Debiagi et al. [46]. However, as the latter study lacks reaction enthalpies, their values were incorporated from Gentile et al. [32]. The RAC (Ranzi-Anca-Couce) scheme has been applied from the work of Anca-Couce et al. [54], and the parameters of secondary charring were obtained from Anca-Couce and Scharler [53]. However, as opposed to the originally described scheme, the formation reaction of dehydrated sugars (levoglucosan and xylan) was included, so the values of x_{CELL} and x_{HCE} parameters have been increased appropriately, although subjectively (Table 2). In Table S3 a list of appropriately grouped compounds covered by the detailed kinetic schemes (Ranzi and RAC scheme), along with their molar masses and molecular formulas, is shown.

3.2.2. Temperature prediction accuracy

Initially, the accuracy of the models was assessed by fitting the simulated centre temperature profile and the experimental profile (fig. 5). The focus was not only on obtaining a quantitative fit (R^2 for data between 100 s and 600 s), but also on the accuracy of capturing the shape of the experimental temperature profile, which contains a plateau between 250 s and 350 s (with a temperature between

350 °C and 400 °C), and a peak around 400 s (temperature above 420 °C). Literature indicates that the plateau is related to the degradation of hemicellulose and cellulose (holocellulose) and the evaporation of its decomposition products [19, 94, 95]. As pointed out by Di Blasi et al. [94, 96], for pyrolysis at temperatures below ca. 500 °C, the reaction enthalpy in the central part of the particle is the driver of the peak in temperature. There are several theories regarding the cause of the occurrence of this peak [94], assigning it to the degradation of lignin or attributing it to the heat of condensation reactions of the carbon structures associated with the metaphase (polycondensation of the basic structural units (BSUs)) [95, 97-101].

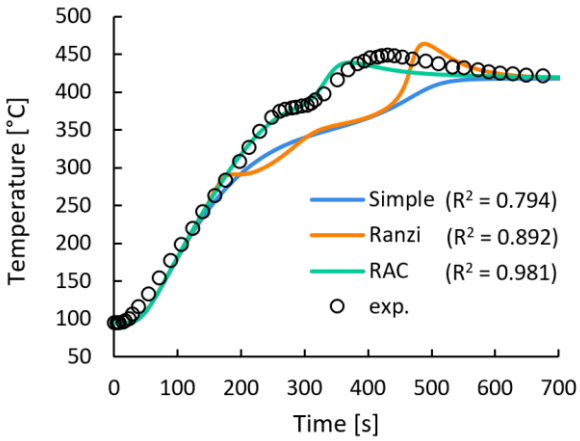

Fig. 5. Simulated centre temperature profiles using different kinetic schemes (Simple, Ranzi and RAC), validated with experimental data (exp.) from Bennadji et al. [55].

The simple scheme and the Ranzi scheme showed strong under-prediction of temperature in the range related to the degradation of hemicellulose (below 300 °C) and cellulose (around 350 °C) (fig. 5). The Ranzi and RAC kinetic scheme, as opposed to the simple kinetic scheme, simulated the exothermal peak. However, the peak location and its shape obtained from the Ranzi scheme did not agree with the experimental data. The determination coefficients of fit (R^2) of the centre's temperature between 100 s and 600 s (time of conversion) for the simple, Ranzi and RAC scheme were 0.794, 0.892 and 0.981, respectively. Overall, the RAC model was able to simulate the temperature profile with much higher accuracy, and its prediction of the temperature peak location and its shape was satisfactorily

precise. Considering the similar origin of both detailed kinetic schemes and the application of the same thermo-physical parameters, the strong deviation in model-predicted temperature profiles was unexpected. The Ranzi and RAC schemes differ in the reactions accounted for, degradation products considered and the kinetic parameters, while the greatest difference between both kinetic schemes was in the reaction enthalpies.

3.2.3. Reaction enthalpies in the kinetic schemes and their relevance

For the Ranzi scheme, the total thermal outcome of the pyrolysis reaction (exo/endothermicity) changes rapidly with the conversion degree, and for the RAC scheme, the overall thermal outcome is consistently exothermic, despite the degradation of cellulose showing significant endothermicity (fig. 6). The complete conversion as predicted by the model with the Ranzi scheme implemented was c.a. 100 s later than for the model where the RAC scheme was used. The secondary degradation of hemicellulose in the Ranzi scheme is strongly endothermic and creates a significant heat sink that lowers the heating rate, and in consequence, leads to the appearance of the first semi-plateau (change in slope) on the temperature profile (between 150 s and 250 s). Such a semi-plateau at 418 °C obtained with the Ranzi scheme was also observed in the work of Corbetta et al. [31]. In the RAC scheme, conversion of the hemicellulose is considered entirely exothermic, so a resulting hemicellulose-related temperature plateau was not observed. On the opposite, for the Ranzi model, the hemicellulose-related heat sink is evident, hence the plateau was visually pronounced. The presence of the hemicellulose-related heat sink influences the subsequent degradation rate of cellulose. It can be observed in fig. 6 as the difference between both kinetic schemes in the location and duration of the cellulose-related semi-plateau.

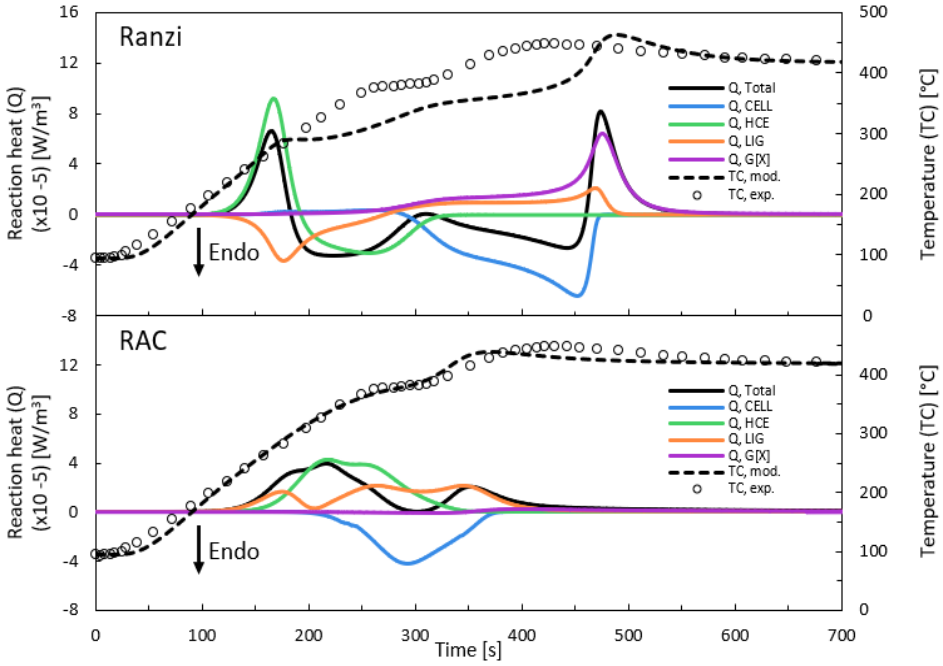

Fig. 6. Model-predicted degradation reaction enthalpies of the lumped bio-components (left axis) and the centre temperature (right axis) using the Ranzi and RAC kinetic scheme, compared with data from Bennadji et al. [55] (Q – reaction heat, Total – all bio-components, CELL – celluloses, HCE – all hemicelluloses, LIG – lignins, G[X] – metaphase, TC – temperature of centre, mod. – simulated profile, exp. – experimental profile).

The time of appearance and shape of the exothermic peak also differs significantly between kinetic schemes, which is related to the reaction enthalpies of metaphase degradation. The Ranzi scheme contains a strong heat release with the degradation of the trapped CO_2 and CO, which constitutes a major share of the heat that creates the peak. In the RAC scheme, the values for those heats were significantly reduced at the investigated temperature because they have barely reacted, so the heat creating the peak is provided mostly by lignin degradation (fig. 8). Such an approach is in agreement with experimental works [50, 102, 103]. It shows that reactions at slightly higher temperatures than the investigated here lead to a further exothermicity, which could be associated with the carbonaceous material devolatilisation or BSU's re-organization, so mainly provided by the G[X] forms as in the RAC model.

The fast pyrolysis process described by the Ranzi scheme occurs in the kinetic regime (small particles, unhindered volatile release), which differs significantly from the conversion in the thermally thick regime (large particles, hindered volatile release). When the release of the heavy volatile compounds (e.g., levoglucosan, xylan) is restricted, the compounds cannot evaporate efficiently from the internal surface and partially undergo heterogeneous conversion into lighter compounds and char [47-50]. The reaction enthalpy increases almost linearly with the increase in restricting the volatiles release, hence char formation [7, 94, 104], while the formation and evaporation of heavy volatiles have an endothermic effect [94]. In the RAC scheme, the inhibition of the volatiles release is taken into account by the secondary charring parameters "x". These parameters alter the kinetic path of conversion and the reaction enthalpies, resulting in less endothermic degradation of the bio-components and greater compatibility with the experimental results of wood conversion in the thermally thick regime.

3.2.4. Yields of lumped products and compounds release profiles

Pyrolysis products were lumped into 3 groups (according to Table S3): the sum of the char and metaphase (C+CM) being designated as the char yield, the sum of the water, light and heavy condensables (CD+T+W) being designated as bio-oil yield and the sum of the permanent gases (PG) being indicated as pygas yield. The numerical error in closing the mass balance for each model was negligible (< 2 wt. %), and each kinetic scheme predicted yields of lumped pyrolysis products fairly well (fig. 9). The simple scheme overpredicted bio-oil yield (by 5 wt. %) at the expense of the char yield. The Ranzi model noticeably overpredicted the pygas yield (by 7 wt. %) and underpredicted the bio-oil and char yield (by 4.5 wt. % and 2.5 wt. %, respectively). The RAC scheme overpredicted the bio-oil (by 3 wt. %) and pygas (by 2 wt. %) yield, underpredicting the char yield. Strangely, for the Ranzi scheme, the combined yields of char and pygas were 8 wt. % higher than for the RAC scheme in which secondary charring was implemented. It is suspected that the enhancement of the char and pygas formation in the Ranzi model is related to the lower predicted heating rates due to the more endothermic hemicellulose conversion.

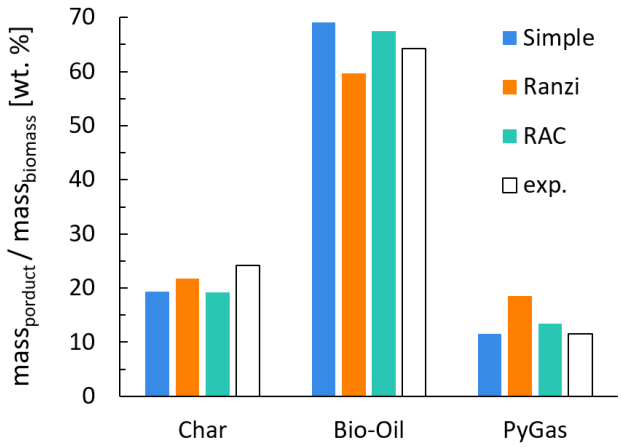

Fig. 7. Simulated pyrolysis yields obtained using the Simple, Ranzi and RAC kinetic scheme compared to the experimental data (exp.) from 418 °C by Bennadji et al. [55].

The model developed by Gentile et al. [32] was based on the experimental data from Cobretta et al. [31], so data was acquired in the same research group as in Bennadji et al. [55]. The similar origin of the experimental data on which the model is based allows for a direct comparison of the results of the Ranzi scheme from this study (fig. 8) with the vapour/gas release profile results of Gentile et al. [32]. Such analysis is beneficial, because it provides insights into the performance of the Ranzi kinetic scheme and may reveal the influence of the recent modifications to the scheme, such as the RAC scheme [31, 32, 46]. Only the release profiles of CO_2, CO and methanol obtained with the Ranzi scheme in this study and in Gentile et al. present high similarity [32]. The release profile of CH_4 obtained by Gentile et al. shows underprediction by this studies' model, especially in the later stage of conversion, while this studies' model data indicate strong overprediction in the initial stage [32]. The problem with a premature release of the methane in the simulations with the detailed kinetic models in comparison to experimental data was already noticed in literature [49, 54]. Nonetheless, its origin is still not clear. For formaldehyde, there is a proper fit in the initial stage, however, the model appears to underpredict the later stages of release, as it is also observed in Gentile et al. [32]. Interestingly, in models using the older Ranzi scheme [31, 32], the experimentally obtained acetic acid release matched the release of hydroxyacetaldehyde (HAA), so a comparison of the acetic acid release profile could not be made. Since acetic acid was firstly incorporated into the scheme by Debiagi et al. [46], it is suspected that

hydroxyacetaldehyde was selected in place of acetic acid as the formation of the latter was assumed not to be significant in the older scheme [31, 32].

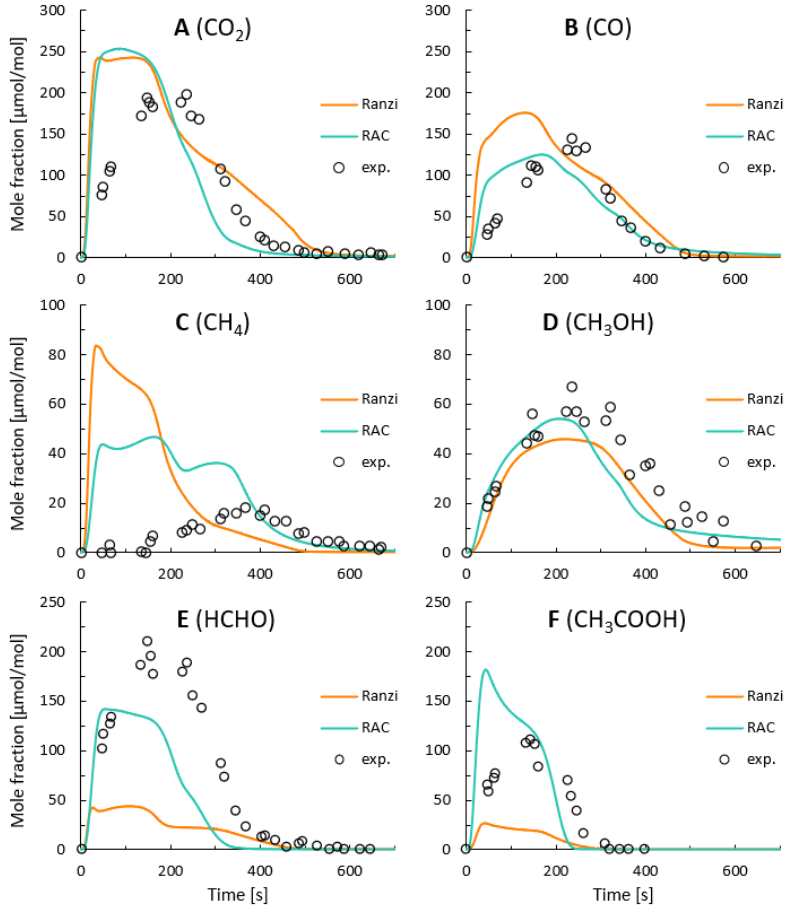

Fig. 8. Simulated compounds release profiles obtained with the Ranzi and RAC kinetic scheme and data (exp.) from Bennadji et al. [55] (A – CO_2, B – CO, C – CH_4, D – methanol (CH_3OH), E – formaldehyde (HCHO), F – acetic acid (CH_3COOH)).

Overall, the compound release profiles obtained in this study with the Ranzi scheme are comparable to other modelling studies [31, 32]. So, the current model with the Ranzi scheme can be assessed as reproducible despite not being able to accurately predict the experimental release profiles of all compounds considered. Unfortunately, for the results obtained with the model including the RAC scheme, a similar comparison cannot be made as for the Ranzi scheme, as modelling results of pyrolysis of a single wood particle using the RAC scheme were not yet available in the literature. Although, for indirect comparison, the results from a pyrolysis model of a single wood pellet with implemented RAC

scheme could be used [54]. Due to differences in the structure of the kinetic schemes, the predictions obtained by the Ranzi and the RAC scheme showed a deviation in compounds (fig. 8). Both schemes show overprediction in the release of the CO_2, CO and CH_4 in the initial stage of the conversion (up to 200 s), most noticeably for the latter compound. However, in the later stages of the conversion, the model-predicted release profile of the gases fitted well with the experimental data (figs 8A, 8B, 8C). The evolution of methanol is well predicted by both models (fig. 8D). For the formaldehyde and acetic acid, the Ranzi scheme significantly underpredicted their release in comparison to the RAC scheme (figs 8E, 8F).

The model incorporating the simple kinetic scheme is fairly accurate in predicting the temperature profile and yields of lumped products, but it does not allow to study of the release of the individual vapour/gas-phase compounds. Therefore, simple schemes should not be applied for advanced model-based investigation of pyrolysis. The model incorporating the RAC scheme showed higher accuracy in the simulation of the temperature profile in comparison to the model using the Ranzi scheme. The RAC scheme implements a restriction on the release of the gas and vapour compounds, hence altering the degradation pathway and reaction enthalpy associated with it, which has high relevance for the conversion of larger particles. Moreover, results from the model based on the RAC scheme are in better agreement with the experimental data (Bennadji et al. [55]) for the yields of lumped products and release profiles of formaldehyde and acetic acid when compared to models based on the Ranzi scheme. Therefore, for the conversion of a wood particle in the thermally thick regime, the use of the RAC scheme is deemed more suitable. Nevertheless, the RAC model is based on the application of the secondary charring parameters ("x") being currently subjectively selected before the simulation. As such, a quantitative correlation between the degree of conversion and secondary charring parameters needs to be established to remove manual fitting bias from the scheme's accuracy. Here it is needed to mention that the lack of implementing the catalytic effect of the AAEMs may be one of the factors that cause the discrepancy between experimental and simulated results regardless of the applied kinetic scheme. The catalytic influence of the alkali and alkaline earth metals, AAEMs (especially

potassium), was neglected in the presented study, but those elements can influence the conversion pathway, conversion yields as well as thermal effect of the conversion [105-111] . So far, the effect has not been incorporated into the reaction scheme nor validated (despite several attempts) [105, 107, 108, 112, 113], so it could not be implemented in the developed models. Therefore, the Ranzi and RAC scheme is only validated for, so restricted to biomasses with very low AAEMs content (like stem wood). For biomasses more burdened with mineral matter, the model's extension with the catalytic influence needs to be made to become validated.

3.3. Model reliability at variable pyrolysis temperature, particle size and shape

3.3.1. Foundations of models

This section presents results from models from Part 3, which include the assessment whether the appropriately established models can simulate the pyrolysis process in a single particle over a broad range of process conditions (temperature, particle size and shape). Moreover, this Part investigates the dependency between process parameters and the heating rate occurring within the particle during conversion. The models were constructed and validated with experimental results from Atreya et al. [33]. For the model-based investigation in this section, only data for cylinders and spheres were used from the aforementioned study (yielding in total 24 scenarios). Models of one shape (12 scenarios) were computed simultaneously in parallel mode with the use of the High-Performance Computing facility at UGent. That reduced computation time from 144 h = 6 days (computation in series) to 12 h (computation in parallel) for 12 scenarios (1 shape) (details in the Supplementary Information, Section S3). The specific model parameters of the wood cylinder were selected in accordance with the experiments conducted by Atreya et al. [33], which next were used to simulate the experimental conditions for models of Part 3 are shown in Table 3. The listed boundary temperatures in the table indicate specific scenarios that were available in the experimental study, and which were used as validation data. The averaged values, along with the standard deviation of the boundary temperatures,

were obtained by averaging the temperatures within one temperature scenario for all sizes of particles within the same shape.

Table 3. Specific parameters used in Part 3 models in accordance with the work of Atreya et al. [33] (longitudinal direction on the z-axis and the radial direction on the r-axis). The different temperatures and particles diameters indicate a specific scenario being modelled (boundary temperatures variation related to the average of all scenarios with a specific temperature for all particles with a certain shape).

Parameter	Symbol	Unit	Value
Particle	Cylinder/Sphere, dry maple wood		
Diameters	$D1/D1$ $D2/D2$ $D3/D3$	[mm]	10/10 15/15 20/20
Height	$H/-$	[mm]	20/-
Moisture content	MC	[wt. %]	0
Bulk density (dry)	$< \rho_S >$	[kg/m^3]	630
Bio-components conc.			
Cellulose (CELL)	c_{CELL}	[wt. %]	42.20
Hemicellulose (HCE)	c_{HCE}	[wt. %]	32.30
H-rich lignin (LIG-H)	c_{LIGH}	[wt. %]	16.51
O-rich lignin (LIG-O)	c_{LIGO}	[wt. %]	5.59
C-rich lignin (LIG-C)	c_{LIGC}	[wt. %]	3.30
Thermal conductivity			
Biomass (Longitudinal)	$\lambda_{Biomass,z}$	[W/(m·K)]	0.255
Biomass (Radial)	$\lambda_{Biomass,r}$	[W/(m·K)]	0.115
Char (Longitudinal)	$\lambda_{Char,z}$	[W/(m·K)]	0.105
Char (Radial)	$\lambda_{Char,r}$	[W/(m·K)]	0.081
Permeability			
Biomass (Longitudinal)	$K_{Biomass,z}$	[m^2]	$1 \cdot 10^{-14}$
Biomass (Radial)	$K_{Biomass,r}$	[m^2]	$1 \cdot 10^{-16}$
Char (Longitudinal)	$K_{Char,z}$	[m^2]	$5 \cdot 10^{-13}$
Char (Radial)	$K_{Char,r}$	[m^2]	$5 \cdot 10^{-14}$
Boundary temperatures			
Gas	$T_{Gas,500\,°C}$ $T_{Gas,610\,°C}$ $T_{Gas,720\,°C}$ $T_{Gas,840\,°C}$	[°C]	494 ± 13 603 ± 6 714 ± 8 838 ± 18
Wall	$T_{Wall,500\,°C}$ $T_{Wall,610\,°C}$ $T_{Wall,720\,°C}$ $T_{Wall,840\,°C}$	[°C]	509 ± 13 618 ± 6 726 ± 8 850 ± 18
Initial	T_{Ini}	[°C]	40

The parameters that were not provided in the referenced study were selected from the literature. Wood density was selected from Park et al. [27], and the thermal conductivity of wood and char was selected from Lee et al. [93]. However, the thermal conductivities in the radial direction for wood and its derived char were increased by 10% (subjectively selected to enhance accuracy) on similar bases as in Part 2 [31, 67, 79, 80]. Also, the permeability values were applied accordingly, as in Part 2 (Section 3.2). The initial concentration of bio-components was used from Park et al. [27], and split parameters were used from Cobretta et al. [31]. The samples were dried prior to the pyrolysis in the experiments, so the moisture content was neglected, and the drying sub-models were not implemented.

For the kinetic scheme, the RAC scheme was applied for all scenarios. Implementing the secondary charring parameters as a single set of constants for all simulated scenarios (Table 3) did not allow obtaining the required accuracy due to significant variation in the conversion conditions (along with the different scenarios) in terms of pyrolysis temperature and particles size. Therefore, the secondary charring parameters were implemented as simple functions with a variable related to a specific scenario, as presented in Table 4. It needs to be pointed out here, that the function was calibrated by iterative simultaneous simulation of the 12 scenarios (4 temperatures x 3 sizes x 1 shape = cylinder), until the correlation function did lead to an accurate result for all 12 scenarios. Details can be found in Section S6.3. in the Supplementary Information.

Table 4. Secondary charring parameters in relation to scenario-specific process conditions ($R_{\parallel}$ - in mm, T_{END} in °C).

Parameter	Unit	Relation	Applied range	Limit ($0 < x$)
x_{CELL}	[-]	$0.016\,R_{\parallel} - 0.02$	$5 \leq R_{\parallel} \leq 10$	$R_{\parallel} < 1.25$
x_{HCE}	[-]	$0.016\,R_{\parallel} + 0.06$	$5 \leq R_{\parallel} \leq 10$	$No\ limit$
x_{LIG}	[-]	$0.565 - 0.00053\,T_{END}$	$480 \leq T_{END} \leq 870$	$1065 < T_{END}$
$x_{G[X]}$	[-]	$0.565 - 0.00053\,T_{END}$	$480 \leq T_{END} \leq 870$	$1065 < T_{END}$

In preliminary simulations, an investigation was made to find the most appropriate relationship between the set parameters of a model and the secondary charring parameter, which results in the highest fit of the centre temperature and mass loss profile to experimental data. Initially, the relation was based on only one set parameter (boundary temperature) for all charring factors, however, that did not lead to promising results, and an additional set parameter (size of a particle) had to be taken into account. Satisfactory results were obtained when the secondary charring parameter of cellulose (x_{CELL}) and hemicellulose (x_{HCE}) were made dependent on the particle size, and the lignin (x_{LIG}) and metaphase ($x_{G[X]}$) charring parameters were expressed as a function of pyrolysis temperature. The particle size parameter was selected as the longest distance between the particle's centre and surface in the direction in which fibres have parallel alignment ($R_{\parallel}$), so the radius in all investigated cases. The pyrolysis temperature parameter was selected as the equilibrium temperature of the centre after completed conversion (i.e. after the exothermal peak), so when the stable temperature was reached at the end of the conversion process (T_{END}) equal to the expected temperature of pyrolysis.

3.3.2. Performance of the model over a broad range of parameters

Validation of the model results with the experimental data from Atreya et al. [33] shows that the model predicted the centre temperature and mass loss with more than satisfactory accuracy considering the broad range of process conditions applied (cylinders in fig. 9, and spheres in fig. S7). For all models simulating pyrolysis at 500 °C, the presence of the exothermic peak was observed, and such a peak faded with an increase in pyrolysis temperature. It is in agreement with literature reports [94, 96]. Simulations of the centre temperature profile at 500 °C showed a good fit for the initial and later stage of conversion, however, only for particles with a diameter of 10 and 15 mm. For both cylinders and spheres with a diameter of 20 mm, the centre temperature profile showed only a satisfactory fit in the initial stage of conversion. Simulations with pyrolysis temperature above 500 °C presented a lack of fit in the initial stages of the conversion. The discrepancy between simulation and experiment increased

with particle size and was more noticeable in spheres than in the cylindrical particles. However, in the later stages of conversion, the profiles showed a very good match with the experimental data.

Even with the implementation of the secondary charring parameters as functions, the misfit in the initial stage of conversion in simulations with pyrolysis temperatures above 500 °C was evident (especially at 840 °C). This suggests that the discrepancy can be related to the modelled heat transfer (its parameters or description) besides the implemented kinetic scheme. The pre-trial simulations showed that a significant increase in the radial thermal conductivity led to a reduction in the initial misfit. However, such a change also implied a strong overprediction of temperature in the later stages of the conversion and the overall temperature profile's shape. Therefore, a major adjustment of thermal conductivity did not have a beneficial effect on fitting the temperature profile and cannot be treated as a general solution to improve the calibration of the current models. Moreover, this parameter is set for well-defined cases (when wood thermal conductivity is measured prior to the experimental work), so it cannot be used for adjustment or calibration. The problem with the initial misfit in the temperature profile seems to have a much more complex foundation besides the thermal conductivity. That involves issues with the radiative heat transfer within the particle (for scenarios with the temperature above 500 °C) and dynamic changes in heat transfer distance due to the shrinking of the particle. The influence of the dynamically changing particle size (i.e., shrinking of the particle especially prevalent in the later stage of conversion) was not accounted for since the particle's shrinking behaviour was not implemented into the model, so its role cannot be objectively stated. Sources indicate that a single particle can undergo cracking during pyrolysis (especially if the particle exceeds 4 mm size), which could influence the temperature profile. On the other hand, none of the sources indicates at exactly which stage of conversion (time, temperature) the cracking occurs. However, it is suspected that it occurs mainly at the end of the conversion due to the pressure build-up at the particle's centre [27, 114]. Nonetheless, the referenced study does not mention the occurrence of fragmentation of particles, so the extent of particle cracking as a contributing factor remains unknown [33]. Another factor that cannot be ruled out is the influence of the experimental

setup in the course of the conversion (e.g., heating through the thermocouple). It could explain the noticeable difference in the temperature profile between particles with 10/15 mm and 20 mm. However, in the experimental setup, thermocouples with a diameter of 0.25 mm were used to assess the temperature in the particle centre, which suggests that the heating through such narrow thermocouples should rather not have an influence [27, 33].

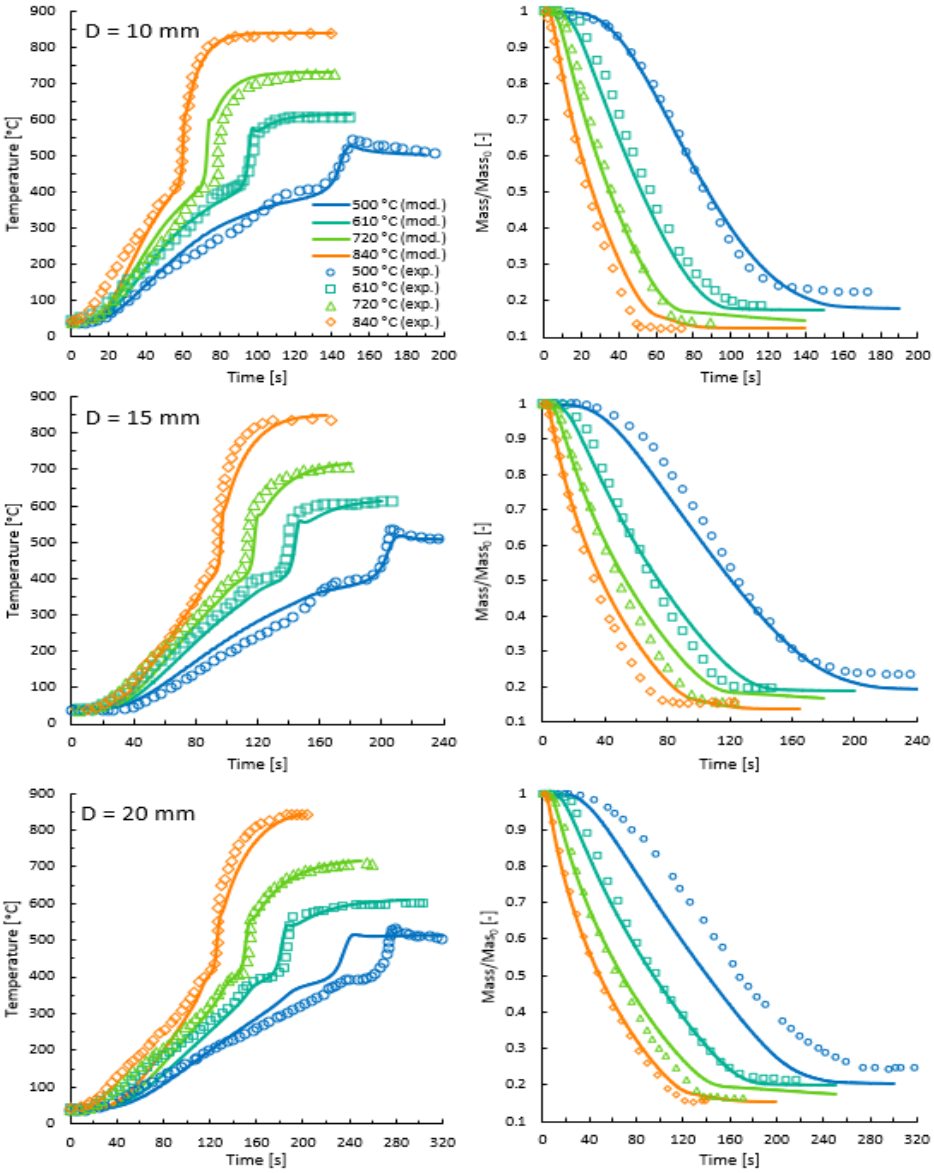

Fig. 9. Temperature centre (TC) and mass loss (ML) profiles from simulation (mod.) for pyrolysis at 500 °C, 610 °C, 720 °C and 840 °C for wood cylinders with 20 mm height and various diameters, and data (exp.) from Atreya et al. [33] (Left - TC, Right - ML).

Due to the small error in mass balance (for every scenario < 5 wt. %), the models can be assessed as unburdened with numerical error. The experimental results did not include release profiles of specific compounds or total yields of lumped products such as bio-oil or non-condensable gases, so only char yield was available for use as validation data (fig. 10) [33]. For spheres, the absolute error between predicted and experimental char yield was 1.3 ± 0.7 wt. %. For cylinders, the error was a bit higher (1.8 ± 1.5 wt. %) due to the low accuracy of simulations at 500 °C (in which there was an error of 4.2 ± 0.2 wt. %). In general, among all simulations, those at 500 °C showed the lowest prediction accuracy with respect to mass loss (fig. 9 and fig. S7) and to final char yield for all particles sizes considered (fig. 10). However, the accuracy improved majorly with an increase in pyrolysis temperature. It is suspected that the inaccuracy of the mass loss profile and char yield prediction in simulations at 500 °C may be related to an inappropriate formulation of the functions describing the secondary charring parameters. Therefore, the relation between the charring parameters and pyrolysis at lower temperatures needs to be further investigated to simulate the process with higher precision. Nonetheless, the results from 500 °C for spheres are strangely much more accurate than for cylinders. In comparison to the data available in the literature (e.g., Wang et al. [23]), it can be noticed that the results for the cylinders from Atreya et al. at 500 °C show a slightly lower char yield [33]. However, the source of the difference between the studies remains inconclusive.

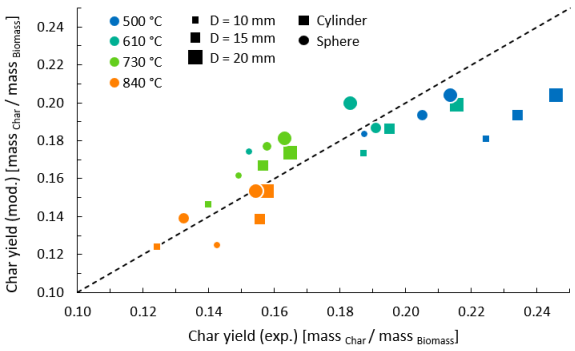

Fig. 10. Experimental [33] and simulated char yields for particles pyrolysed in temperatures between 500 °C and 840 °C (squares – cylinders, circle: spheres).

For simulations at 720 °C and 840 °C, up until halfway through the conversion, their predicted mass loss profiles showed an excellent agreement with the experimental profiles, but along the course of the conversion, the profiles lose their precise fit (fig. 9 and fig. S7). The overprediction of char yield for both particle shapes occurred mainly for simulations at 720 °C but not at 840 °C (fig. 10). The omission of gasification reactions ([88-91]) in the model seems not to be a factor affecting inaccuracy in the later stage of the conversion since the effect of gasification reactions (if significant) would lead to an opposite trend. Therefore, suboptimal kinetics describing the metaphase degradation up to 720 °C are suspected as the major cause behind the lack of fit in the mass loss profiles in the later stages of conversion. Overall, the models show satisfactory validity in the given validation scenarios, so further analysis is considered to be reliable.

For modelling release profiles and yields of specific compounds in pyrolysis of wood at elevated temperatures in a realistic manner (T > 500 °C [54] or T > 650 °C [31]), secondary gas-phase reactions have to be incorporated. These reactions occur within the particle and after the release of volatiles in the volume surrounding the particle. The surrounding volume is required to be included in the model to reliably account for these secondary reactions [31, 54]. The models in this study did not simulate the volume which surrounds the particle, so secondary gas-phase reactions were omitted. Hence, yields of the lumped products (heavy and light condensable (T and CD), permanent gases (PG) and water (W)) are based only on the RAC's primary kinetic scheme and its relationship with the process conditions. A comparison of the yields of the lumped products from scenarios with different process conditions is shown in fig. 11, and the data show noticeable similarity to the experimental data from fluidised bed pyrolysis [23, 114, 115]. The overview of the results is presented in Section S9.4. in the Supplementary Information.

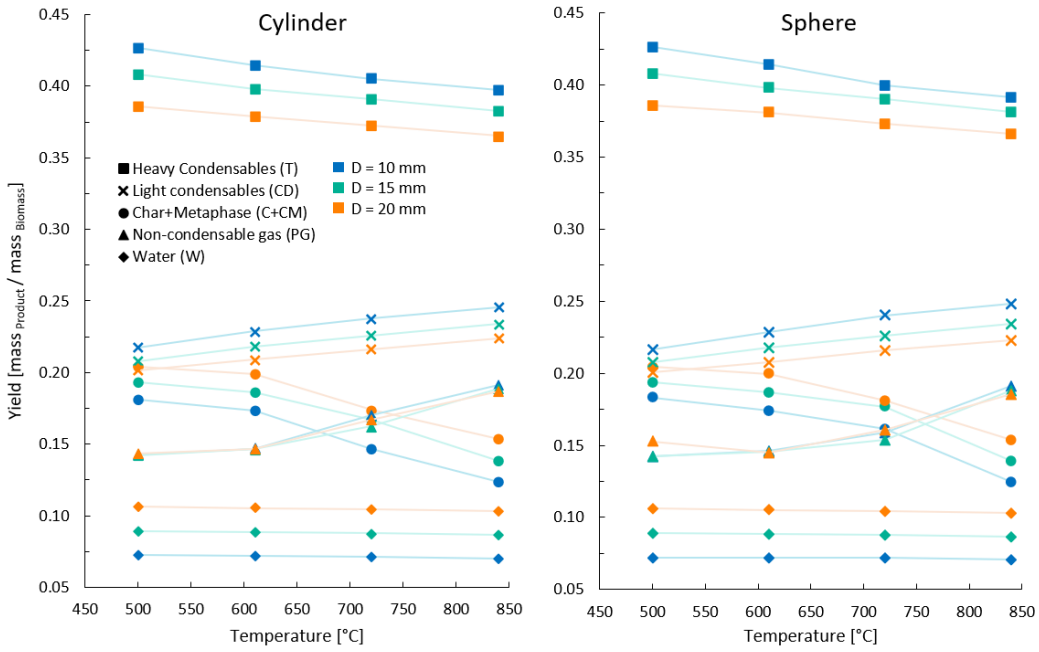

Fig. 11. Model-predicted lumped yields of pyrolysis products as a function of temperature (500 °C, 610 °C, 720 °C and 840 °C), particle size (D = 10 mm, 15 mm and 20 mm) and shape (Left - cylinder, Right - sphere).

The secondary charring parameters were implemented as linear functions of the particles size for both particle shapes. However, changes in yields of pyrolysis products with the particle's size for the same shape as well as between shapes are not linear (fig. 11). Therefore, it is assumed that the heating rate, besides the secondary charring parameters, is another conversion-wise relevant parameter that influences the pyrolysis yields. Hence, two factors, heating rate and secondary charring parameters, also have to be taken into account to explain the observed differences in the linearity of changes in the pyrolysis yields. Overall, the structure of the models allowed to obtain results that were positively validated with the experimentally obtained profiles, hence results from these models can be assessed as very reliable and satisfactorily accurate. Basing on the obtained outcome from models, the influence of temperature, size and shape on the simulation outcome can be investigated.

3.3.3. Outer thermal layer

Only the heating rate that occurs during the conversion has a direct relation to the path of conversion. Therefore, averaged values of the heating rate as a function of the conversion extent at specific particle locations were used in this investigation instead of values averaged over the entire simulation time (the latter being the more common practice). From the heating rate distribution, it can be observed that its value is not evenly distributed among the whole domain of the particle. Therefore, specific points within the particles were selected to assess the influence of the pyrolysis temperature and particle size on the heating rate. Details of the assessment on the cylindrical particle are presented in Supplementary Information (Section S9.5.).

How much the heating rate changed (and the linearity thereof) with temperature was majorly dependent on the location within the particle. The most noticeable increase in heating rate was on the line between the centre point and the edge of the cylinder's base, although the radial direction was more influenced than the longitudinal. The cause of the latter may be related to higher thermal conductivity and a stronger cooling effect (higher permeability) in the longitudinal direction, as investigated in Part 1 (Section 3.1). The relative radial position of the investigated points was set constant, so with an increase in particle size, the absolute distance from the investigated point to the surface differed (which is also the case for the points at the particle's centre). The absolute distance between the point and the surface was the main factor causing differences in heating rate in the longitudinal and radial direction. Therefore, if the point in the spatial body is located sufficiently far from the surface, the heating rate during the conversion is not significantly influenced by the pyrolysis temperature. The largest changes in heating rate with pyrolysis temperature occur in the layer closest to the surface.

Independent of the heating rate, the existence of a pattern was noticed on volatile release profiles at the particle surface, e.g., for heavy condensables (T) shown in fig. 12. For all particles pyrolysed at 840 °C, from the start till approx. 30 s, the model-predicted release profiles are in very good agreement

with each other. Also, the value of the maximum model-predicted mass flux (0.017 kg/(m^2·s)) and the time of its appearance (8 s) is very similar for all scenarios (840 °C). After the initial match of release profiles, the mass flux profiles start to differ in the further stage of conversion, and they become dependent on the shape and size of each modelled particle. A similar outcome was obtained for pyrolysis of wood cylinders above 650 °C in the experimental study by Gauthier et al. [116]. Analysis of results shows that for the first 30 s, the same volume of all particles was converted in a very similar manner, which confirms the existence of the outer thermal layer with comparable thickness for every simulated scenario.

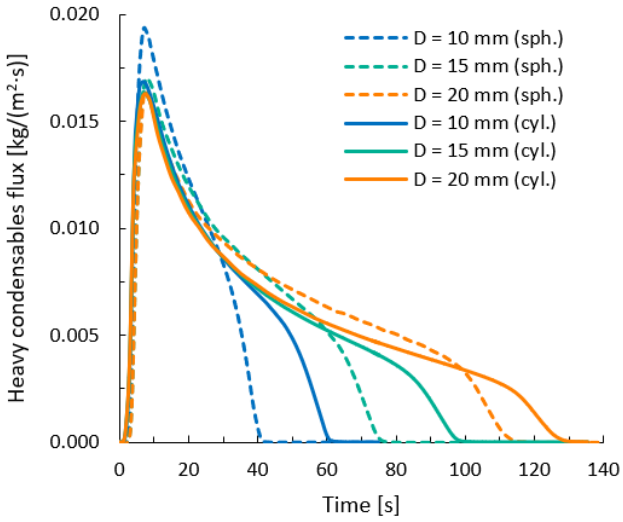

Fig. 12. Simulated surface mass fluxes of heavy condensables for cylindrical and spherical particles with different sizes (D = 10 mm, 15 mm and 20 mm) at a pyrolysis temperature of 840 °C.

Analysis of the simulated heating rate distribution indicated that only the outer approx. 2.5 mm of the particle is prone to drastically change its heating rate as affected by pyrolysis temperature (further referred as the outer thermal layer). At 500 °C, the thermal layer is hardly noticeable, but with an increase in pyrolysis temperature, its presence becomes more recognisable, and at 840 °C, its thickness is sharply visible (fig. 13). Interestingly, the thickness of the outer layer was independent of the particle size. Although, the shape had an influence on the heating rate within the layer due to the dependency of inward thermal flux and surface area per volume to which the flux is directed. The relevance of the

thermal outer layer on the heating rate distribution depends on the magnitude of the thermal flux and the thermal resistivity. Moreover, it is suspected that the thickness of the layer is related to the thermophysical parameters of wood (via thermal resistivity), so it can vary for different species. With a presumed constant thickness of this thermal layer, a change in particle size leads to an increase in the volume ratio between the layer and the inner volume. For the cylindrical particles, the ratios were 4.3, 2.0 and 1.4, and for spheres 7.0, 2.4 and 1.4, both for D = 10 mm, 15 mm and 20 mm, respectively. A higher value of this ratio indicates that a higher share of particle mass is converted at significantly higher heating rates than in other parts of the particle. The existence of the outer thermal layer would explain the changes in the linearity of the simulated yields of lumped pyrolysis products versus temperature. Basing on the results obtained from the primary kinetic scheme, the observed trend can be indicated as: the lower the value of thermal layer volume/inner volume ratio (so for large particles), the higher the yields of char (C+CM) and water (W) and the lower the yields of heavy and light condensables (T and CD). Nonetheless, in a more general view, the pyrolysis temperature and implemented kinetic scheme (secondary charring parameters) may have a more significant influence than the outer layer itself. Considering that observations enclosed in this Section are numerically based, their validation with experimental data is required.

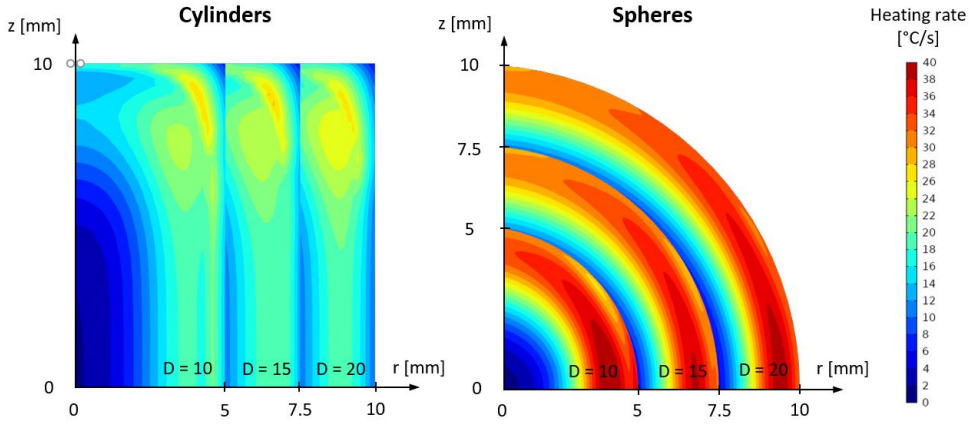

Fig. 13. Simulated heating rate distribution at a pyrolysis temperature of 840 °C for cylindrical (left) and spherical (right) particles at the 8th second of the conversion (merged view for 3 sizes of particles: D = 10 mm, 15 mm and 20 mm).

The obtained results indicate the presence of the outer layer of the particles with c.a. 2.5 mm thickness in all investigated cases for all modelled particles, which behave similarly despite differences in particle shape and size. The consequence of this thermal layer's presence is a significantly higher heating rate close to the particle's surface in comparison to the inner volume of the particle. Therefore, through the size of a particle, the heating rate has the ability to cause a noticeable influence on the pyrolysis yields. The implication of the numerically observed thermal layer will be that the restriction for efficient conversion of a wood particle with a high heating rate, its size should not exceed 4 – 5 mm in any direction. The literature does not contain sufficient reference data from single particle pyrolysis to assess the implementation's reliability objectively. However, studies of the pyrolysis of wood particles in fluidised beds indicate the correctness of this implication [23, 114, 115, 117]. The references studies indicate the existence of 3 particle size ranges within which particle's conversion occurs differently. Considering the char yield, it can be stated that up to 1 mm, increasing the particle size results in an increase in char yield. Then, between 1 mm and 3 - 4 mm, the char yield remains relatively constant, but above 4 mm, with an increase in size, the char yield increases again (logarithmically). Therefore, for particles in the middle size range, the conversion occurs ratter homogeneously in the whole particle volume, presumably with the same heating rate at any location within a particle. Then with a larger size, the effect of the thermal layer may become more pronounced. Besides the size of the particle, the conversion and its yields (as well as the significance of the suspected thermal layer) can be altered by other parameters of conversion like temperature, or vapours residence time and experimental setup/reactor type [114, 115, 118-120]. Therefore, a conclusive statement in regard to the influence and presence of the thermal layer must be made with extreme caution.

3.4. Future improvements in models for single wood particle pyrolysis in the thermally thick regime

Despite the generally good agreement among the models and experimental data, the results in fig. 9 and fig. S4 show that the misfit in the temperature profile is located in a different stage of the conversion than where discrepancies in the mass loss profile occur. This is an indication that models, despite their satisfactory accuracy, still do not fully resemble the actual conversion taking place in single wood particles. The conversion takes place in the thermally thick regime, so all processes that influence the heat transfer have relevance and need to be accurately implemented and interconnected. Within the heat transfer model, along with its sub-models and parameters on which they are based, an indication of several areas where an improvement is required and will be discussed briefly hereafter. Considering the variety of multi-coupled factors, improvements need to be comprehensive and be done with precision and carefulness. It needs to be reminded, that the parameters of the real system cannot be freely changed in the model description since they are strictly related to the actual properties of a material. The only changes that should be made (and are in principle allowed) are the descriptions of the sub-model which are implemented.

The description of effective thermal conductivity plays a major role in heat transfer, so its appropriate implementation has high importance. The simplest and most commonly used formulation is one provided by Grønli [26]. Literature also provides other formulations dedicated especially to wood [79, 121-123]. The detailed formulation was provided by Thunman and Leckner [64], based on merged approaches from Siau [122] and Saastamoinen and Richard [123]. The dedicated formulation seems to be a better fit for the purpose, but there are a few concerns regarding its use. The formulation is based on wood porosity and thermal conductivity of a single, non-porous fibre (perpendicular and parallel direction). Thunman and Leckner proposed one set of values, which should be valid for every type of wood, but considering the variation of the bio-composition in wood, the formulation may not be appropriate for all wood species [64]. Moreover, the authors propose thermal conductivity values of wood char “fibre” based on coal, which in their own opinion, can be inaccurate. Therefore, as long as

the thermal conductivity values for wood and biochar are not reliable, the use of this formulation by Thunman and Leckner cannot be advised. The implementation of Grønli's formulation of effective thermal conductivity requires the use of the thermal conductivities of materials (wood, char) that are highly corresponding to the modelled scenario (specie, density, and for the char, pyrolysis temperature) [26]. For a specific wood, the values of the thermal conductivity can be found in the literature (Longitudinal (n = 25) – Min. = 0.25 W/(m K), Max. = 0.45 W/(m K), Avg. ± St. Dev. = 0.33 ± 0.05; Radial (n = 25) – Min. = 0.09, Max. = 0.31, Avg. ± St. Dev. = 0.18 ± 0.06) [18, 124, 125]. For wood chars, the situation is much more difficult because only a few studies provided those parameters, and that includes only for a few species (Longitudinal (n = 13) – Min. = 0.11 W/(m K), Max. = 0.34W/(m K), Avg. ± St. Dev. = 0.24 ± 0.07; Radial (n = 13) – Min. = 0.03, Max. = 0.13, Avg. ± St. Dev. = 0.08 ± 0.03) [80, 93], and data for char does not match wood species or modelled conditions. As pointed out in Section 3.3.2., manual calibration of the thermal conductivity of wood and char may not be sufficient or even beneficial for model performance.

The formulation of effective thermal conductivity consists of conductive heat transfer in solids and voids and internal radiative transfer, which above 500 °C has a non-negligible share. In literature, several descriptions of radiative transfer can be found [13, 126-129]. Nevertheless, predictions on their basis differ significantly for the same temperature and pore size (fig. S12). For future development, it would be beneficial to assess their accuracy and choose one on an objective basis. An additional difficulty in the implementation of the radiative heat transfer is the use of the appropriate pore width in wood char. In literature, reliable data on the shape and dimensions of the vessels/lumens in specific wood species can be found [6, 79, 130, 131]. However, the changes in the width of the wood pores during pyrolysis have not been described yet, and the literature is not abundant with the pore width measurements in wood chars. Also, considering that for both hard and softwoods, the size of a lumen in the longitudinal direction is close to 1000 times higher than in the radial or tangential direction, it needs to be assessed if the assumption of the isotropic radiative transfer has validity [6].

The heat transfer is also connected to the true density and porosity. In the investigated models, as well as in other studies [6, 27, 28, 31-33, 43, 54-57], the value of the true density of the solid is set as constant, but the experimental studies on chars indicate a change of true density with temperature [132-134]. To accurately implement changes in bulk density, besides the appropriate function of the true density, the model has to be extended with an accurate description of shrinking [32, 61, 63, 135]. Both features have to be implemented simultaneously, considering their compensatory effect on overall porosity within the modelled domain. The compensatory effect may be one of the causes why some studies indicate the low relevance of the shrinking [61]. As pointed out in Section 3.3.3, only when particle shrinking is implemented, dynamic changes in distance are taken into account, and the heat transfer is described in accordance with reality. However, the effects are negligible for particles below 1 mm and become more pronounced when the particle size or temperature increases [62].

Implementing the anisotropic gas permeability is often neglected in studies [27, 31-33, 35, 54]. Nevertheless, the lack of appropriately implementing gas permeability leads to a suboptimal prediction of pressure within the particle, hence the gas velocity distribution within the particle and intrinsic residence time of vapours. The latter has severe consequences for the secondary gas-phase reactions, confirmed experimentally and numerically [30, 31]. Also, as shown in Section 3.1.2., the permeability influences the heating rate distribution through the convective cooling effect, especially when the particles were initially moist. A similar problem with thermal conductivity has to be solved for the gas permeability, namely, how it dynamically changes with temperature. The experimental data for chars of various wood species is also lacking. An additional problem is posed by the strong deficit in validation datasets, like pressure profiles within particles. Due to very complex measurements, only a few studies provide pressure profiles of wood particles during pyrolysis [93].

When heat transfer is implemented in a reliable manner along with case-specific thermo-physical parameters and bio-composition corresponding to the validation dataset (e.g., [48, 49]), the model can be used for finding adjustments to the detailed kinetic schemes. With reliable changes in the heating

rate and pressure distribution, the detailed kinetic schemes can be investigated and improved, but only at pyrolysis temperatures below which the secondary gas-phase reactions are negligible. For a wood particle, the dependence of reaction kinetics on the heat transfer is described by the dimensionless pyrolysis (Py) and Biot (Bi) numbers. Considering that woods differ in thermo-physical properties only within certain limits, both dimensionless numbers depend mainly on the pyrolysis temperature and characteristic length related to the particle size [8-11]. However, the dimensionless numbers are only an approximation by averaging the conversion characteristics, which in the case of large particles can have a different course depending on the location within the particle's domain. As presented in Section 3.3.3., the conversion in close vicinity to the particle's surface compared to the conversion in the geometric centre can differ substantially, despite the whole particle having single values for the dimensionless numbers. Therefore, direct global correlations of conversion based on Py and Bi numbers, hence assigning the whole large particle into one kinetic regime, may lead to model inaccuracy. Therefore, a more appropriate and accurate solution has to be found. To avoid the subjective selection of parameter values for the secondary charring factors in the RAC scheme, they should be coupled with the heating rate, the partial vapour pressure of specific compounds and concentration of available catalytically active sites on which the secondary reactions take place [47]. This will also open up the possibility of reliable adjustment of the reaction enthalpies in the primary kinetic scheme. Moreover, numerous studies show that the concentration of the alkali and alkaline earth elements (AAEMs) influences the degradation of initial bio-components (via alteration of activation energy and pre-exponential factor and the reaction heat of formation of specific volatiles) [105, 108-111, 136, 137]. Nonetheless, severe caution needs to be taken to prepare a study that aims to identify their effect. The first issue is the appropriate selection of the dopant (i.e., inorganic element) concentration to match the concentration of the elements in stem wood. The second, when leaching of the biomass is applied to produce demineralized biomass, also the changes in the bio-composition of the biomass (extractive content, degradation of hemicellulose) due to the use of the leaching agent (i.e., acid) have to be considered. For the latter, it is also important to assure that the leaching agent

was removed from the material prior to doping or processing [106, 107, 109, 138] . Then, based on the appropriately prepared study, an attempt to introduce a modification to the kinetic scheme can be provided, and a quantitative correlation of the effect of catalytically active elements on the kinetic parameters and thermal effects can be proposed [107, 108, 112, 113]. When a detailed pyrolysis scheme consistently includes the effect of inorganics, it will be meaningful to study its influence in a particle model, as done in this work with the currently available detailed pyrolysis schemes. That, in the end, would extend the validity of the Ranzi and RAC scheme to feedstock more burdened with mineral matter than stem wood (like herbaceous biomass).

For adjustment of the kinetic scheme at temperatures in which secondary gas-phase reactions are no longer negligible, it is necessary to extend the particle model with the surrounding (external) volume, along with an appropriate description (mass and heat transfer and fluid flow in the surrounding volume). Then, depending on the modelled temperature, the model has to be completed with the following reactions: thermal cracking of vapours, reactions between vapours and gases, steam gasification and Boudouard reaction. However, first, an assessment of the kinetic parameters for secondary cracking of volatiles has to be performed to indicate their appropriate value to be used in the single particle models [14, 92].

4. Conclusions

As presented, the modelling of pyrolysis of a single wooden particle in the thermally thick conversion regime is a complex and demanding task and requires high caution from the modeller with the selection of parameters and formulation of specific sub-parts of the model. The step-by-step approach presented in this work allowed to state that:

- The influence of anisotropy in thermal conductivity, hence the difference in model outcome (with respect to assuming isotropy), could not be accurately assessed as the obtained differences in mass loss and temperatures between the models were in the range of the deviations in the

experimental results. However, the implementation of anisotropy in wood has high relevance for accurate simulation of the distribution of intrinsic gas velocity, hence the retention time of vapours within a particle and secondary reactions of vapours. Therefore, implementation of the directional dependence of parameters is advised when the previous processes are of interest.

- For the higher dimensional models with appropriate implementation of the parameters and sub-model description, the performance of the kinetic, equilibrium and heat sink model for the description of drying is highly similar. If the particle is well-assessed experimentally (thermal conductivity and permeability), the most appropriate model for the description of the drying is the equilibrium model due to its realistic description of the phenomenon. Otherwise, as is commonly the case, the selection of less realistic, but still precise models like the kinetic or heat sink model can be implemented. Moreover, the heat sink model is preferred to the kinetic model since the sub-optimal selection of the parameters in the kinetic model leads to a higher risk of low precision than for the heat sink model.
- Among investigated detailed kinetic schemes, the implementation of the RAC kinetic scheme led to the most accurate results in terms of the parameter profiles and overall yields in the conducted study. It also presented the most reliable reaction heats. Therefore, the implementation of the RAC model for the description of wood pyrolysis in the thermally thick regime is advised.
- A well-established single particle model is able to predict the centre temperature and mass loss profile fairly accurately within a broad range of process parameters (pyrolysis temperature, particle size and shape). However, to increase its precision, the secondary charring parameters in the RAC kinetic scheme have to be related to relevant parameters. Correlations proposed in this work are based on temperature and particle size for the investigated conditions. They should be extended in the future to consider other parameters such as the heating rate or the presence of inorganics.
- Simulations indicated the presence of the outer thermal layer which thickness (ca. 2.5 mm) was the same for all particles despite varying size and shape. Therefore, it suggests that homogeneous

efficient heating of particles can be made only if their size does not exceed 4 - 5 mm. However, this result has to be validated experimentally.

In the future, additional improvements have to be implemented into the model to obtain the required precision of prediction. It will require the development in both the model description as well as a broader and more detailed experimental dataset for validation purposes. Then, the well-established pyrolysis model of a single wood particle will allow for in-depth investigation of the relationship between wood properties and process conditions occurring during the conversion. That, in the end, will open a possibility for further technological optimisation of pyrolysis-based processes using biomass as feedstock and a more conscious approach to tailoring of the large-scale process. Then, the well-established pyrolysis model of a single wood particle will allow for in-deep investigation of the relationship between wood properties and process conditions occurring during the conversion, which at the moment, are poorly understood. Moreover, the well-developed single particle model will provide a baseline, from which the influence of the reactor could be distinguished and then separately optimised. Finally, that will open a possibility for further technological optimisation of pyrolysis-based processes using biomass as feedstock and a more conscious approach to tailoring the large-scale process.

Declaration of Competing Interest

The authors declare that they have no known competing financial interests or personal relationships that could have appeared to influence the work reported in this paper.

CRediT authorship contribution statement

Przemyslaw Maziarka – Conceptualization, Methodology, Investigation, Software, Formal analysis, Visualisation, Writing - Original Draft; **Andrés Anca-Couce** – Conceptualization, Writing - Review & Editing; **Wolter Prins** – Writing - Review & Editing; **Frederik Ronsse** - Supervision, Conceptualization, Funding acquisition, Writing - Review & Editing

Acknowledgements

The authors would like to thank UGent's High-Performance Computing centre (HPC-UGent) for providing the computing resources. We would also like to express our sincere gratitude to Kenneth Hoste for his invaluable help with the configuration of the software on the infrastructure and troubleshooting the connection issues.

Funding

This research was funded by the GreenCarbon. The GreenCarbon project has received funding from the European Union's Horizon 2020 research and innovation programme under the Marie Skłodowska-Curie grant agreement No 721991.

References

[1] F. Sebastián, J. Royo, M. Gómez, Cofiring versus biomass-fired power plants: GHG (Greenhouse Gases) emissions savings comparison by means of LCA (Life Cycle Assessment) methodology, Energy 36 (2011) 2029-2037.
[2] H. de Coninck, A. Revi, M. Babiker, P. Bertoldi, M. Buckeridge, A. Cartwright, W. Dong, J. Ford, S. Fuss, J.-C. Hourcade, D. Ley, R. Mechler, P. Newman, A. Revokatova, S. Schultz, L. Steg, T. Sugiyama, Strengthening and Implementing the Global Response. In: Global Warming of 1.5°C. An IPCC Special Report on the impacts of global warming of 1.5°C above pre-industrial levels and related global greenhouse gas emission pathways, in the context of strengthening the global response to the threat of climate change, sustainable development, and efforts to eradicate poverty, in: V. MassonDelmotte, P. Zhai, H.-O. Pörtner, D. Roberts, J. Skea, P.R. Shukla, A. Pirani, W. Moufouma-Okia, C. Péan, R. Pidcock, S. Connors, J.B.R. Matthews, Y. Chen, X. Zhou, M.I. Gomis, E. Lonnoy, T. Maycock, M. Tignor, and T. Waterfield (Ed.) IPCC - The Intergovernmental Panel on Climate Change 2018, pp. 313 - 443.
[3] S.J. Gerssen-Gondelach, D. Saygin, B. Wicke, M.K. Patel, A.P.C. Faaij, Competing uses of biomass: Assessment and comparison of the performance of bio-based heat, power, fuels and materials, Renewable and Sustainable Energy Reviews 40 (2014) 964-998.
[4] G. Dubois, Modeling and simulation: challenges and best practices for industry, CRC Press, Boca Raton, 2018.
[5] M. Himmel, M. Tucker, J. Baker, C. Rivard, K. Oh, K. Grohmann, Comminution of biomass: hammer and knife mills, John Wiley, New York, 1986, pp. 39-58.
[6] P.N. Ciesielski, M.F. Crowley, M.R. Nimlos, A.W. Sanders, G.M. Wiggins, D. Robichaud, B.S. Donohoe, T.D. Foust, Biomass Particle Models with Realistic Morphology and Resolved Microstructure for Simulations of Intraparticle Transport Phenomena, Energy & Fuels 29 (2015) 242-254.
[7] A. Anca-Couce, Reaction mechanisms and multi-scale modelling of lignocellulosic biomass pyrolysis, Progress in Energy and Combustion Science 53 (2016) 41-79.
[8] K. Van Geem, Chapter 6 - Kinetic modeling of the pyrolysis chemistry of fossil and alternative feedstocks, in: T. Faravelli, F. Manenti, E. Ranzi (Eds.) Computer Aided Chemical Engineering, Elsevier2019, pp. 295-362.
[9] D.L. Pyle, C.A. Zaror, Heat transfer and kinetics in the low temperature pyrolysis of solids, Chemical Engineering Science 39 (1984) 147-158.
[10] M.S. Mettler, D.G. Vlachos, P.J. Dauenhauer, Top ten fundamental challenges of biomass pyrolysis for biofuels, Energy & Environmental Science 5 (2012) 7797-7809.
[11] A.D. Paulsen, M.S. Mettler, P.J. Dauenhauer, The Role of Sample Dimension and Temperature in Cellulose Pyrolysis, Energy & Fuels 27 (2013) 2126-2134.
[12] C. Di Blasi, Analysis of Convection and Secondary Reaction Effects Within Porous Solid Fuels Undergoing Pyrolysis, Combustion Science and Technology 90 (1993) 315-340.
[13] A.M.C. Janse, R.W.J. Westerhout, W. Prins, Modelling of flash pyrolysis of a single wood particle, Chemical Engineering and Processing: Process Intensification 39 (2000) 239-252.
[14] C. Di Blasi, Modeling chemical and physical processes of wood and biomass pyrolysis, Progress in Energy and Combustion Science 34 (2008) 47-90.
[15] M. Jalili, A. Anca-Couce, N. Zobel, On the Uncertainty of a Mathematical Model for Drying of a Wood Particle, Energy & Fuels 27 (2013) 6705-6717.
[16] I. Haberle, N.E.L. Haugen, Ø. Skreiberg, Drying of Thermally Thick Wood Particles: A Study of the Numerical Efficiency, Accuracy, and Stability of Common Drying Models, Energy & Fuels 31 (2017) 13743-13760.
[17] I. Haberle, Ø. Skreiberg, J. Łazar, N.E.L. Haugen, Numerical models for thermochemical degradation of thermally thick woody biomass, and their application in domestic wood heating appliances and grate furnaces, Progress in Energy and Combustion Science 63 (2017) 204-252.

[18] P. Maziarka, F. Ronsse, A. Anca-Couce, Review on Modelling Approaches Based on Computational Fluid Dynamics for Biomass Pyrolysis Systems, in: Z. Fang, R.L. Smith Jr, L. Xu (Eds.) Production of Biofuels and Chemicals with Pyrolysis, Springer Singapore, Singapore, 2020, pp. 373-438.
[19] M.B. Pecha, J.I.M. Arbelaez, M. Garcia-Perez, F. Chejne, P.N. Ciesielski, Progress in understanding the four dominant intra-particle phenomena of lignocellulose pyrolysis: chemical reactions, heat transfer, mass transfer, and phase change, Green Chemistry 21 (2019) 2868-2898.
[20] P.N. Ciesielski, M.B. Pecha, A.M. Lattanzi, V.S. Bharadwaj, M.F. Crowley, L. Bu, J.V. Vermaas, K.X. Steirer, M.F. Crowley, Advances in Multiscale Modeling of Lignocellulosic Biomass, ACS Sustainable Chemistry & Engineering 8 (2020) 3512-3531.
[21] A. Cuoci, Chapter 13 - Numerical modeling of reacting systems with detailed kinetic mechanisms, in: T. Faravelli, F. Manenti, E. Ranzi (Eds.) Computer Aided Chemical Engineering, Elsevier2019, pp. 675-721.
[22] S.R.A. Kersten, X. Wang, W. Prins, W.P.M. van Swaaij, Biomass Pyrolysis in a Fluidized Bed Reactor. Part 1: Literature Review and Model Simulations, Industrial & Engineering Chemistry Research 44 (2005) 8773-8785.
[23] X. Wang, S.R.A. Kersten, W. Prins, W.P.M. van Swaaij, Biomass Pyrolysis in a Fluidized Bed Reactor. Part 2: Experimental Validation of Model Results, Industrial & Engineering Chemistry Research 44 (2005) 8786-8795.
[24] G.L. Comstock, Directional permeability of softwoods, Wood and Fiber Science 4 (1970) 283-289.
[25] A.J. Stamm, Wood and cellulose science, Ronald Press Co., New York, USA, 1964.
[26] M.G. Grønli, A theoretical and experimental study of thermal degradation of biomass (Ph.D. Thesis), Mechanical Engineering, NTNU, Trondheim, Norway, 1996, pp. 258.
[27] W.C. Park, A. Atreya, H.R. Baum, Experimental and theoretical investigation of heat and mass transfer processes during wood pyrolysis, Combustion and Flame 157 (2010) 481-494.
[28] A. Anca-Couce, N. Zobel, Numerical analysis of a biomass pyrolysis particle model: Solution method optimized for the coupling to reactor models, Fuel 97 (2012) 80-88.
[29] C. Brackmann, M. Aldén, P.-E. Bengtsson, K.O. Davidsson, J.B.C. Pettersson, Optical and Mass Spectrometric Study of the Pyrolysis Gas of Wood Particles, Applied Spectroscopy 57 (2003) 216-222.
[30] P. Maziarka, P. Sommersacher, X. Wang, N. Kienzl, S. Retschitzegger, W. Prins, N. Hedin, F. Ronsse, Tailoring of the pore structures of wood pyrolysis chars for potential use in energy storage applications, Applied Energy 286 (2021) 116431.
[31] M. Corbetta, A. Frassoldati, H. Bennadji, K. Smith, M.J. Serapiglia, G. Gauthier, T. Melkior, E. Ranzi, E.M. Fisher, Pyrolysis of Centimeter-Scale Woody Biomass Particles: Kinetic Modeling and Experimental Validation, Energy & Fuels 28 (2014) 3884-3898.
[32] G. Gentile, P.E.A. Debiagi, A. Cuoci, A. Frassoldati, E. Ranzi, T. Faravelli, A computational framework for the pyrolysis of anisotropic biomass particles, Chemical Engineering Journal 321 (2017) 458-473.
[33] A. Atreya, P. Olszewski, Y. Chen, H.R. Baum, The effect of size, shape and pyrolysis conditions on the thermal decomposition of wood particles and firebrands, International Journal of Heat and Mass Transfer 107 (2017) 319-328.
[34] X. Shi, F. Ronsse, J.G. Pieters, Finite element modeling of intraparticle heterogeneous tar conversion during pyrolysis of woody biomass particles, Fuel Processing Technology 148 (2016) 302-316.
[35] P.O. Okekunle, T. Pattanotai, H. Watanabe, K. Okazaki, Numerical and Experimental Investigation of Intra-Particle Heat Transfer and Tar Decomposition during Pyrolysis of Wood Biomass, Journal of Thermal Science and Technology 6 (2011) 360-375.
[36] X. Shi, J. Gao, X. Lan, Modeling the Pyrolysis of a Centimeter-Sized Biomass Particle, Chemical Engineering & Technology 42 (2019) 2574-2579.
[37] L. Forest Products, Wood handbook : wood as an engineering material, (2010).
[38] M.P. Olszewski, S.A. Nicolae, P.J. Arauzo, M.-M. Titirici, A. Kruse, Wet and dry? Influence of hydrothermal carbonization on the pyrolysis of spent grains, Journal of Cleaner Production 260 (2020) 121101.

[39] N. Dahmen, E. Henrich, E. Dinjus, F. Weirich, The bioliq® bioslurry gasification process for the production of biosynfuels, organic chemicals, and energy, Energy, Sustainability and Society 2 (2012) 3.
[40] Food, N. Agriculture Organization of the United, B. Mechanical Wood Products, Industrial charcoal making, Food and Agriculture Organization of the United Nations, Rome, 1985.
[41] C. Di Blasi, E.G. Hernandez, A. Santoro, Radiative Pyrolysis of Single Moist Wood Particles, Industrial & Engineering Chemistry Research 39 (2000) 873-882.
[42] A. Galgano, C. Di Blasi, Modeling the propagation of drying and decomposition fronts in wood, Combustion and Flame 139 (2004) 16-27.
[43] H. Lu, W. Robert, G. Peirce, B. Ripa, L.L. Baxter, Comprehensive Study of Biomass Particle Combustion, Energy & Fuels 22 (2008) 2826-2839.
[44] F. Shafizadeh, P.P.S. Chin, Thermal Deterioration of Wood, in: I.S. Goldstein (Ed.) Wood Technology: Chemical Aspects, American Chemical Society, Washington D.C., USA, 1977, pp. 57-81.
[45] E. Ranzi, A. Cuoci, T. Faravelli, A. Frassoldati, G. Migliavacca, S. Pierucci, S. Sommariva, Chemical Kinetics of Biomass Pyrolysis, Energy & Fuels 22 (2008) 4292-4300.
[46] P. Debiagi, G. Gentile, A. Cuoci, A. Frassoldati, E. Ranzi, T. Faravelli, A predictive model of biochar formation and characterization, Journal of Analytical and Applied Pyrolysis 134 (2018) 326-335.
[47] J. Rath, M.G. Wolfinger, G. Steiner, G. Krammer, F. Barontini, V. Cozzani, Heat of wood pyrolysis, Fuel 82 (2003) 81-91.
[48] N. Lang, C. Rupp, H. Almuina-Villar, A. Dieguez-Alonso, F. Behrendt, J. Röpcke, Pyrolysis behavior of thermally thick wood particles: Time-resolved characterization with laser based in-situ diagnostics, Fuel 210 (2017) 371-379.
[49] H. Almuina-Villar, A. Anca-Couce, N. Lang, J. Ropcke, F. Behrendt, A. Dieguez-Alonso, Laser-Based Spectroscopy Diagnosis and Detailed Numerical Models to Gain Understanding on the Slow Pyrolysis Behavior of Thermally Thick Wood Particles, Chemical Engineering Transactions, 65 (2018) 109-114.
[50] N. Zobel, A. Anca-Couce, Influence of intraparticle secondary heterogeneous reactions on the reaction enthalpy of wood pyrolysis, Journal of Analytical and Applied Pyrolysis 116 (2015) 281-286.
[51] J.R. Jones, Q. Chen, G.D. Ripberger, Secondary Reactions and the Heat of Pyrolysis of Wood, Energy Technology 8 (2020) 2000130.
[52] A. Anca-Couce, R. Mehrabian, R. Scharler, I. Obernberger, Kinetic scheme of biomass pyrolysis considering secondary charring reactions, Energy Conversion and Management 87 (2014) 687-696.
[53] A. Anca-Couce, R. Scharler, Modelling heat of reaction in biomass pyrolysis with detailed reaction schemes, Fuel 206 (2017) 572-579.
[54] A. Anca-Couce, P. Sommersacher, R. Scharler, Online experiments and modelling with a detailed reaction scheme of single particle biomass pyrolysis, Journal of Analytical and Applied Pyrolysis 127 (2017) 411-425.
[55] H. Bennadji, K. Smith, S. Shabangu, E.M. Fisher, Low-Temperature Pyrolysis of Woody Biomass in the Thermally Thick Regime, Energy & Fuels 27 (2013) 1453-1459.
[56] H. Bennadji, K. Smith, M.J. Serapiglia, E.M. Fisher, Effect of Particle Size on Low-Temperature Pyrolysis of Woody Biomass, Energy & Fuels 28 (2014) 7527-7537.
[57] H. Lu, E. Ip, J. Scott, P. Foster, M. Vickers, L.L. Baxter, Effects of particle shape and size on devolatilization of biomass particle, Fuel 89 (2010) 1156-1168.
[58] Z. Zeng, R. Grigg, A Criterion for Non-Darcy Flow in Porous Media, Transport in Porous Media 63 (2006) 57-69.
[59] S.V. Vassilev, C.G. Vassileva, Y.-C. Song, W.-Y. Li, J. Feng, Ash contents and ash-forming elements of biomass and their significance for solid biofuel combustion, Fuel 208 (2017) 377-409.
[60] C. Telmo, J. Lousada, N. Moreira, Proximate analysis, backwards stepwise regression between gross calorific value, ultimate and chemical analysis of wood, Bioresource Technology 101 (2010) 3808-3815.
[61] M. Bellais, K.O. Davidsson, T. Liliedahl, K. Sjöström, J.B.C. Pettersson, Pyrolysis of large wood particles: a study of shrinkage importance in simulations☆, Fuel 82 (2003) 1541-1548.

[62] K.M. Bryden, M.J. Hagge, Modeling the combined impact of moisture and char shrinkage on the pyrolysis of a biomass particle☆, Fuel 82 (2003) 1633-1644.
[63] G. Caposciutti, H. Almuina-Villar, A. Dieguez-Alonso, T. Gruber, J. Kelz, U. Desideri, C. Hochenauer, R. Scharler, A. Anca-Couce, Experimental investigation on biomass shrinking and swelling behaviour: Particles pyrolysis and wood logs combustion, Biomass and Bioenergy 123 (2019) 1-13.
[64] H. Thunman, B. Leckner, Thermal conductivity of wood—models for different stages of combustion, Biomass and Bioenergy 23 (2002) 47-54.
[65] M.N. Özisik, Heat conduction, (1993).
[66] H. Fatehi, X.S. Bai, A Comprehensive Mathematical Model for Biomass Combustion, Combustion Science and Technology 186 (2014) 574-593.
[67] K. Raznjevic, Handbook of thermodynamic tables and charts, Hemisphere Publishing, Washington D.C., USA, 1976.
[68] F. Thurner, U. Mann, Kinetic investigation of wood pyrolysis, Industrial & Engineering Chemistry Process Design and Development 20 (1981) 482-488.
[69] V. Mamleev, S. Bourbigot, M. Le Bras, J. Yvon, The facts and hypotheses relating to the phenomenological model of cellulose pyrolysis: Interdependence of the steps, Journal of Analytical and Applied Pyrolysis 84 (2009) 1-17.
[70] M. Nowakowska, O. Herbinet, A. Dufour, P.-A. Glaude, Detailed kinetic study of anisole pyrolysis and oxidation to understand tar formation during biomass combustion and gasification, Combustion and Flame 161 (2014) 1474-1488.
[71] M. Asmadi, H. Kawamoto, S. Saka, Thermal reactivities of catechols/pyrogallols and cresols/xylenols as lignin pyrolysis intermediates, Journal of Analytical and Applied Pyrolysis 92 (2011) 76-87.
[72] A. Cuoci, T. Faravelli, A. Frassoldati, S. Granata, G. Migliavacca, E. Ranzi, A general mathematical model of biomass devolatilization. Note 1. Lumped kinetic models of cellulose, hemicellulose and lignin, in: F. Scala (Ed.) Proceedings of the 30th combustion meeting of the Italian Section of the Combustion Institute, ASICI, Milan, 2007, pp. 2.1–2.6.
[73] A. Cuoci, T. Faravelli, A. Frassoldati, S. Granata, G. Migliavacca, S. Pierucci, A general mathematical model of biomass devolatilization. Note 2. Detailed kinetics of volatile species, in: F. Scala (Ed.) Proceedings of the 30th combustion meeting of the Italian Section of the Combustion Institute, ASICI, Milan, 2007, pp. 3.1–3.6.
[74] T. Faravelli, A. Frassoldati, G. Migliavacca, E. Ranzi, Detailed kinetic modeling of the thermal degradation of lignins, Biomass and Bioenergy 34 (2010) 290-301.
[75] E. Ranzi, M. Dente, A. Goldaniga, G. Bozzano, T. Faravelli, Lumping procedures in detailed kinetic modeling of gasification, pyrolysis, partial oxidation and combustion of hydrocarbon mixtures, Progress in Energy and Combustion Science 27 (2001) 99-139.
[76] E. Ranzi, P.E.A. Debiagi, A. Frassoldati, Mathematical Modeling of Fast Biomass Pyrolysis and Bio-Oil Formation. Note I: Kinetic Mechanism of Biomass Pyrolysis, ACS Sustainable Chemistry & Engineering 5 (2017) 2867-2881.
[77] P.E.A. Debiagi, C. Pecchi, G. Gentile, A. Frassoldati, A. Cuoci, T. Faravelli, E. Ranzi, Extractives Extend the Applicability of Multistep Kinetic Scheme of Biomass Pyrolysis, Energy & Fuels 29 (2015) 6544-6555.
[78] A. Anca-Couce, A. Berger, N. Zobel, How to determine consistent biomass pyrolysis kinetics in a parallel reaction scheme, Fuel 123 (2014) 230-240.
[79] T. Maku, Studies on the heat conduction in wood, Wood Research Bulletin, Japan Wood Research Institute, Kyoto University, Kyoto, Japan, 1954, pp. 80.
[80] C.L. Williams, T.L. Westover, L.M. Petkovic, A.C. Matthews, D.M. Stevens, K.R. Nelson, Determining Thermal Transport Properties for Softwoods Under Pyrolysis Conditions, ACS Sustainable Chemistry & Engineering 5 (2017) 1019-1025.
[81] C. Di Blasi, Physico-chemical processes occurring inside a degrading two-dimensional anisotropic porous medium, International Journal of Heat and Mass Transfer 41 (1998) 4139-4150.

[82] S.R.A. Kersten, Biomass gasification in circulating fluidized beds, Twente University Press, Enschede (Netherlands), Netherlands, 2002.
[83] C. Di Blasi, Modeling intra- and extra-particle processes of wood fast pyrolysis, AIChE Journal 48 (2002) 2386-2397.
[84] E.J. Kansa, H.E. Perlee, R.F. Chaiken, Mathematical model of wood pyrolysis including internal forced convection, Combustion and Flame 29 (1977) 311-324.
[85] C. Di Blasi, Heat, momentum and mass transport through a shrinking biomass particle exposed to thermal radiation, Chemical Engineering Science 51 (1996) 1121-1132.
[86] C.D. Blasi, Physico-chemical processes occurring inside a degrading two-dimensional anisotropic porous medium, International Journal of Heat and Mass Transfer 41 (1998) 4139-4150.
[87] P.T. Williams, S. Besler, The influence of temperature and heating rate on the slow pyrolysis of biomass, Renewable Energy 7 (1996) 233-250.
[88] E.E. Kwon, E.-C. Jeon, M.J. Castaldi, Y.J. Jeon, Effect of Carbon Dioxide on the Thermal Degradation of Lignocellulosic Biomass, Environmental Science & Technology 47 (2013) 10541-10547.
[89] C. Xu, S. Hu, J. Xiang, H. Yang, L. Sun, S. Su, B. Wang, Q. Chen, L. He, Kinetic models comparison for steam gasification of coal/biomass blend chars, Bioresource Technology 171 (2014) 253-259.
[90] E.M.A. Edreis, H. Yao, Kinetic thermal behaviour and evaluation of physical structure of sugar cane bagasse char during non-isothermal steam gasification, Journal of Materials Research and Technology 5 (2016) 317-326.
[91] I. Ahmed, A.K. Gupta, Syngas yield during pyrolysis and steam gasification of paper, Applied Energy 86 (2009) 1813-1821.
[92] A. Gómez-Barea, B. Leckner, Modeling of biomass gasification in fluidized bed, Progress in Energy and Combustion Science 36 (2010) 444-509.
[93] C.K. Lee, R.F. Chaiken, J.M. Singer, Charring pyrolysis of wood in fires by laser simulation, Symposium (International) on Combustion 16 (1977) 1459-1470.
[94] C. Di Blasi, C. Branca, F. Masotta, E. De Biase, Experimental Analysis of Reaction Heat Effects during Beech Wood Pyrolysis, Energy & Fuels 27 (2013) 2665-2674.
[95] C. Di Blasi, C. Branca, F.E. Sarnataro, A. Gallo, Thermal Runaway in the Pyrolysis of Some Lignocellulosic Biomasses, Energy & Fuels 28 (2014) 2684-2696.
[96] C. Di Blasi, C. Branca, A. Santoro, E. Gonzalez Hernandez, Pyrolytic behavior and products of some wood varieties, Combustion and Flame 124 (2001) 165-177.
[97] I. Milosavljevic, V. Oja, E.M. Suuberg, Thermal Effects in Cellulose Pyrolysis: Relationship to Char Formation Processes, Industrial & Engineering Chemistry Research 35 (1996) 653-662.
[98] V. Strezov, B. Moghtaderi, J.A. Lucas, Computational calorimetric investigation of the reactions during thermal conversion of wood biomass, Biomass and Bioenergy 27 (2004) 459-465.
[99] M. Becidan, Ø. Skreiberg, J.E. Hustad, Experimental study on pyrolysis of thermally thick biomass residues samples: Intra-sample temperature distribution and effect of sample weight ("scaling effect"), Fuel 86 (2007) 2754-2760.
[100] R. Bilbao, A. Millera, M.B. Murillo, Temperature profiles and weight loss in the thermal decomposition of large spherical wood particles, Industrial & Engineering Chemistry Research 32 (1993) 1811-1817.
[101] J.J. Manyà, J. Ruiz, J. Arauzo, Some Peculiarities of Conventional Pyrolysis of Several Agricultural Residues in a Packed Bed Reactor, Industrial & Engineering Chemistry Research 46 (2007) 9061-9070.
[102] C. Branca, C. Di Blasi, Global Kinetics of Wood Char Devolatilization and Combustion, Energy & Fuels 17 (2003) 1609-1615.
[103] L. Basile, A. Tugnoli, V. Cozzani, Influence of Macrocomponents on the Pyrolysis Heat Demand of Lignocellulosic Biomass, Industrial & Engineering Chemistry Research 56 (2017) 6432-6440.
[104] M.J. Antal, M. Grønli, The Art, Science, and Technology of Charcoal Production, Industrial & Engineering Chemistry Research 42 (2003) 1619-1640.
[105] P. Giudicianni, V. Gargiulo, C.M. Grottola, M. Alfè, A.I. Ferreiro, M.A.A. Mendes, M. Fagnano, R. Ragucci, Inherent Metal Elements in Biomass Pyrolysis: A Review, Energy & Fuels 35 (2021) 5407-5478.

[106] P.R. Patwardhan, J.A. Satrio, R.C. Brown, B.H. Shanks, Influence of inorganic salts on the primary pyrolysis products of cellulose, Bioresource Technology 101 (2010) 4646-4655.
[107] V. Gargiulo, P. Giudicianni, M. Alfè, R. Ragucci, Influence of possible interactions between biomass organic components and alkali metal ions on steam assisted pyrolysis: A case study on Arundo donax, Journal of Analytical and Applied Pyrolysis 112 (2015) 244-252.
[108] J.S. Arora, K.B. Ansari, J.W. Chew, P.J. Dauenhauer, S.H. Mushrif, Unravelling the catalytic influence of naturally occurring salts on biomass pyrolysis chemistry using glucose as a model compound: a combined experimental and DFT study, Catalysis Science & Technology 9 (2019) 3504-3524.
[109] P.S. H. Almuina-Villar, S. Retschitzegger, A. Anca-Couce, A. Dieguez-Alonso, , Combined Influence of Inorganics and Transport Limitations on the Pyrolytic Behaviour of Woody Biomass, Chemical Engineering Transactions, 80 (2020) 73-78.
[110] C. Di Blasi, C. Branca, A. Galgano, Influences of Potassium Hydroxyde on Rate and Thermicity of Wood Pyrolysis Reactions, Energy & Fuels 31 (2017) 6154-6162.
[111] C. Di Blasi, C. Branca, A. Galgano, Role of the Potassium Chemical State in the Global Exothermicity of Wood Pyrolysis, Industrial & Engineering Chemistry Research 57 (2018) 11561-11571.
[112] A. Trendewicz, R. Evans, A. Dutta, R. Sykes, D. Carpenter, R. Braun, Evaluating the effect of potassium on cellulose pyrolysis reaction kinetics, Biomass and Bioenergy 74 (2015) 15-25.
[113] A.I. Ferreiro, M. Rabaçal, M. Costa, P. Giudicianni, C.M. Grottola, R. Ragucci, Modeling the impact of the presence of KCl on the slow pyrolysis of cellulose, Fuel 215 (2018) 57-65.
[114] C. Di Blasi, C. Branca, Temperatures of Wood Particles in a Hot Sand Bed Fluidized by Nitrogen, Energy & Fuels 17 (2003) 247-254.
[115] R.J.M. Westerhof, H.S. Nygård, W.P.M. van Swaaij, S.R.A. Kersten, D.W.F. Brilman, Effect of Particle Geometry and Microstructure on Fast Pyrolysis of Beech Wood, Energy & Fuels 26 (2012) 2274-2280.
[116] G. Gauthier, T. Melkior, M. Grateau, S. Thiery, S. Salvador, Pyrolysis of centimetre-scale wood particles: New experimental developments and results, Journal of Analytical and Applied Pyrolysis 104 (2013) 521-530.
[117] S. Zhou, M. Garcia-Perez, B. Pecha, A.G. McDonald, R.J.M. Westerhof, Effect of particle size on the composition of lignin derived oligomers obtained by fast pyrolysis of beech wood, Fuel 125 (2014) 15-19.
[118] L. Chen, C. Dupont, S. Salvador, G. Boissonnet, D. Schweich, Influence of Particle Size, Reactor Temperature and Gas Phase Reactions on Fast Pyrolysis of Beech Wood, International Journal of Chemical Reactor Engineering 8 (2010).
[119] M. Somerville, A. Deev, The effect of heating rate, particle size and gas flow on the yield of charcoal during the pyrolysis of radiata pine wood, Renewable Energy 151 (2020) 419-425.
[120] C. Di Blasi, C. Branca, V. Lombardi, P. Ciappa, C. Di Giacomo, Effects of Particle Size and Density on the Packed-Bed Pyrolysis of Wood, Energy & Fuels 27 (2013) 6781-6791.
[121] F. Kollmann, L. Malmquist, Über die Wärmeleitzahl von Holz und Holzwerkstoffen, Holz als Roh- und Werkstoff 14 (1956) 201-204.
[122] J.F. Siau, Transport processes in wood, Springer-Verlag, Berlin, Germany, 1984.
[123] J. Saastamoinen, J.-R. Richard, Simultaneous drying and pyrolysis of solid fuel particles, Combustion and Flame 106 (1996) 288-300.
[124] M. J.D., Thermal conductivity of wood, Heat Pip Air Cond 13 (1941) 380–391.
[125] N. Ahn, S. Park, Heat Transfer Analysis of Timber Windows with Different Wood Species and Anatomical Direction, Energies 13 (2020) 15.
[126] H.C. Hottel, A.F. Sarofim, Radiative transfer, McGraw-Hill, New York, 1967.
[127] R.L. Panton, J.G. Rittmann, Pyrolysis of a slab of porous material, Symposium (International) on Combustion 13 (1971) 881-891.
[128] W.-C.R. Chan, M. Kelbon, B.B. Krieger, Modelling and experimental verification of physical and chemical processes during pyrolysis of a large biomass particle, Fuel 64 (1985) 1505-1513.

[129] C. Di Blasi, G. Russo, Modeling of Transport Phenomena and Kinetics of Biomass Pyrolysis, in: A.V. Bridgwater (Ed.) Advances in Thermochemical Biomass Conversion., Springer, Dordrecht, 1994.
[130] M. Plötze, P. Niemz, Porosity and pore size distribution of different wood types as determined by mercury intrusion porosimetry, European Journal of Wood and Wood Products 69 (2011) 649-657.
[131] L. Forest Products, Wood handbook : wood as an engineering material, (2021).
[132] J. Tintner, C. Preimesberger, C. Pfeifer, D. Soldo, F. Ottner, K. Wriessnig, H. Rennhofer, H. Lichtenegger, E.H. Novotny, E. Smidt, Impact of Pyrolysis Temperature on Charcoal Characteristics, Industrial & Engineering Chemistry Research 57 (2018) 15613-15619.
[133] R.A. Brown, A.K. Kercher, T.H. Nguyen, D.C. Nagle, W.P. Ball, Production and characterization of synthetic wood chars for use as surrogates for natural sorbents, Organic Geochemistry 37 (2006) 321-333.
[134] C.E. Brewer, V.J. Chuang, C.A. Masiello, H. Gonnermann, X. Gao, B. Dugan, L.E. Driver, P. Panzacchi, K. Zygourakis, C.A. Davies, New approaches to measuring biochar density and porosity, Biomass and Bioenergy 66 (2014) 176-185.
[135] K.O. Davidsson, J.B.C. Pettersson, Birch wood particle shrinkage during rapid pyrolysis, Fuel 81 (2002) 263-270.
[136] S. Wang, G. Dai, H. Yang, Z. Luo, Lignocellulosic biomass pyrolysis mechanism: A state-of-the-art review, Progress in Energy and Combustion Science 62 (2017) 33-86.
[137] H. Almuina-Villar, N. Lang, A. Anca-Couce, J. Röpcke, F. Behrendt, A. Dieguez-Alonso, Application of laser-based diagnostics for characterization of the influence of inorganics on the slow pyrolysis of woody biomass, Journal of Analytical and Applied Pyrolysis 140 (2019) 125-136.
[138] L. Rodríguez-Machín, L.E. Arteaga-Pérez, J. Vercruysse, R.A. Pérez-Bermúdez, W. Prins, F. Ronsse, Py-GC/MS based analysis of the influence of citric acid leaching of sugarcane residues as a pretreatment to fast pyrolysis, Journal of Analytical and Applied Pyrolysis 134 (2018) 465-475.